

Single-particle excitations in a trapped gas of Fermi atoms in the BCS-BEC crossover region

Y. Ohashi^{1,2} and A. Griffin²

¹*Institute of Physics, University of Tsukuba, Tsukuba, Ibaraki 305, Japan,*

² *Department of Physics, University of Toronto,*

Toronto, Ontario, Canada M5S 1A7

(Dated: July 5, 2018)

arXiv:cond-mat/0410220v1 [cond-mat.other] 8 Oct 2004

Abstract

We investigate the single-particle properties at $T = 0$ of a trapped superfluid gas of Fermi atoms with a Feshbach resonance. A tunable pairing interaction associated with the Feshbach resonance leads to the BCS-BEC crossover, where the character of superfluidity continuously changes from the BCS-type to a BEC of composite bosons (consisting of a superposition of a condensate of Cooper-pairs and molecular bosons). In this paper, we extend our previous work for a uniform superfluid Fermi gas [Y. Ohashi and A. Griffin, *Phys. Rev. A* **67**, 063612 (2003)] to include the effect of a harmonic trap. We do not use the local density approximation (LDA), but directly solve the Bogoliubov-de Gennes coupled equations. Using these equations, we find self-consistent values for the spatially-dependent local density $n(\mathbf{r})$ as well as the composite BCS order parameter $\tilde{\Delta}(\mathbf{r})$, the latter describing both the Cooper-pair and molecular condensate contributions. Using these results, we calculate the single-particle density of states in the crossover region, and from this determine the true single-particle energy gap (E_g) of the trapped Fermi superfluid at $T = 0$. This is associated with the in-gap (or Andreev) states in the low density region at the edge of the trap. We calculate the laser-induced current $I(\omega)$ into another hyperfine state, as measured in recent rf-spectroscopy experiments. This rf-spectrum gives a direct probe of the quasiparticle spectrum. We show how the high-energy part of $I(\omega)$ gives information about $\tilde{\Delta}(r = 0)$ at the center of the trap (which is comparable to the Fermi energy ε_F in the crossover region). More generally, we show that $I(\omega)$ is very dependent on the spatial profile of the pair potential $\tilde{\Delta}(r)$ which is used. We also emphasize that the narrow “unpaired atom” peak in the rf-data gives information about E_g and the low-energy ($\ll \varepsilon_F$) in-gap states of a Fermi superfluid. While our calculations are limited at $T = 0$, we use them to discuss the recent Innsbruck data and the LDA calculations of Törmä and co-workers. The LDA, while useful, can lead to an incorrect physical picture of the low density surface region of the Fermi superfluid.

PACS numbers: 03.75.Ss, 03.75.Kk, 03.70.+k

I. INTRODUCTION

Recently, the BCS-BEC crossover in a trapped gas of Fermi atoms near a Feshbach resonance has attracted much attention[1, 2, 3, 4, 5]. Molecular bosons associated with a Feshbach resonance can mediate a tunable pairing interaction between atoms, which becomes stronger with decreasing threshold energy (denoted by 2ν) of the Feshbach resonance[6, 7]. The BCS-BEC crossover can be studied as a function of 2ν , with the character of superfluidity continuously changing from the conventional BCS-type of Cooper-pairs to a BEC of *composite* bosons (consisting of a superposition of Cooper-pairs and molecules), as one approaches the strong-coupling regime[1, 2, 3, 4]. This situation contrasts with the “classic” crossover physics originally studied in the superconductivity literature [8, 9, 10, 11, 12, 13, 14, 15], where Cooper-pair bosons are always dominant in the whole crossover regime, from the BCS to the BEC limits. Recent experiments on ultracold gases of ^{40}K and ^6Li have used this tunable interaction near the resonance[16, 17], to produce a large number of bound states or molecules when $a_s^{2b} > 0$ (a_s^{2b} is the two-body s -wave scattering length)[18, 19]. Using this tunable interaction, a BEC of these molecular bosons has been observed in ^{40}K and ^6Li [20, 21], and more recently, evidence for superfluidity was found in the BCS side of the crossover regime (loosely defined as $a_s^{2b} > 0$) [22, 23, 24, 25, 26]. Both single-particle excitations[27] and collective modes[25, 28] have been experimentally studied in the crossover regime in the case of ^6Li .

In this paper, we present a detailed study of BCS-type single-particle excitations in the BCS-BEC crossover of a trapped gas of Fermi atoms with a Feshbach resonance. This extends our previous work for a uniform gas[3] in a major way, since we now include the effect of discrete eigenstates due to confinement in a harmonic trap. However, in contrast to Ref.[3], we limit our discussion to $T = 0$ in this paper. Because of the inhomogeneity of a gas due to the trap potential, the single-particle threshold excitation gap E_g is no longer simply related to the position-dependent superfluid pair potential $\tilde{\Delta}(\mathbf{r})$. This contrasts with the case of a uniform Fermi superfluid[3, 9, 12], where E_g and the order parameter $\tilde{\Delta}$ are related in a very direct way ($E_g = |\tilde{\Delta}|$ for $\mu > 0$, $E_g = \sqrt{\mu^2 + |\tilde{\Delta}|^2}$ for $\mu < 0$, where μ is the chemical potential of the fermions). We compute $\tilde{\Delta}(r)$ self-consistently by solving the Bogoliubov-de Gennes (BdG) coupled equations and then use it to calculate the single-particle density of states $N(\omega)$ for a trapped superfluid gas. We present results through the

BCS-BEC crossover by varying the threshold energy 2ν . We also calculate the rf-tunneling current, which can be used to probe the spectrum of the single-particle excitations. We compare our $T = 0$ results with recent experimental data on ${}^6\text{Li}$ [27]. This data agrees with the calculations of Törmä and co-workers[29], using a local density approximation (LDA). While the LDA is useful, we feel that it gives an incorrect picture of the surface region of the trapped superfluid.

This paper is organized as follows: In Sec. II, we introduce the usual coupled fermion-boson Hamiltonian including an isotropic harmonic potential and derive the mean-field BdG equations. The single-particle Green's functions in a trap are expressed in terms of the solutions of the BdG equations in Sec. III. In Sec. IV, we discuss the BCS-BEC crossover in the cases of broad and narrow Feshbach resonances. We review different definitions of the s -wave scattering length. In Sec. V, we calculate the equilibrium properties in a self-consistent way, such as the chemical potential μ (which plays a crucial role), the atomic density profile $n(\mathbf{r})$ and spatial variation of the composite order parameter $\tilde{\Delta}(\mathbf{r})$. The single-particle density of states $N(\omega)$ for different values of 2ν is calculated and discussed in Sec. VI. In Sec. VII, we compare our results (both BdG and LDA) with the rf-tunneling spectroscopy data obtained in recent experiments on ${}^6\text{Li}$. Some of our results were briefly reported earlier in Refs.[30, 31].

II. EXTENSION OF THE BOGOLIUBOV-DE GENNES EQUATIONS ($T = 0$)

We consider a two-component Fermi gas with a Feshbach resonance trapped in a harmonic potential, using the coupled fermion-boson model [1, 2, 3, 4, 6, 7, 32]

$$\begin{aligned}
 H = & \sum_{\sigma} \int d\mathbf{r} \Psi_{\sigma}^{\dagger}(\mathbf{r}) \left[-\frac{\nabla^2}{2m} - \mu + V_{\text{trap}}^{\text{F}}(\mathbf{r}) \right] \Psi_{\sigma}(\mathbf{r}) - U \int d\mathbf{r} \Psi_{\uparrow}^{\dagger}(\mathbf{r}) \Psi_{\downarrow}^{\dagger}(\mathbf{r}) \Psi_{\downarrow}(\mathbf{r}) \Psi_{\uparrow}(\mathbf{r}) \\
 & + \int d\mathbf{r} \Phi^{\dagger}(\mathbf{r}) \left[-\frac{\nabla^2}{2M} + 2\nu - 2\mu + V_{\text{trap}}^{\text{M}}(\mathbf{r}) \right] \Phi(\mathbf{r}) + g_r \int d\mathbf{r} \left[\Phi^{\dagger}(\mathbf{r}) \Psi_{\downarrow}(\mathbf{r}) \Psi_{\uparrow}(\mathbf{r}) + h.c. \right].
 \end{aligned}
 \tag{2.1}$$

Here $\Psi_{\sigma}(\mathbf{r})$ is the fermion field operator with pseudo-spin $\sigma = \uparrow, \downarrow$. The Bose quantum field operator $\Phi(\mathbf{r})$ describes molecular bosons associated with the Feshbach resonance. U is a non-resonant interaction, which we take attractive ($-U < 0$). The Feshbach resonance g_r describes resonance between one molecule and two Fermi atoms. The effect of this resonance

is controlled by adjusting the energy 2ν of the molecules, also referred to as the threshold energy. (To avoid confusion, we note that in many recent papers, this threshold energy is denoted by ν .) Since a molecule consists of two Fermi atoms, we take $M = 2m$ and impose the conservation of the total number of atoms,

$$\begin{aligned} N &= N_F + 2N_M \\ &= \int d\mathbf{r} n_F(r) + 2 \int d\mathbf{r} n_M(r) \\ &= \sum_{\sigma} \int d\mathbf{r} \langle \Psi_{\sigma}^{\dagger}(\mathbf{r}) \Psi_{\sigma}(\mathbf{r}) \rangle + 2 \int d\mathbf{r} \langle \Phi^{\dagger}(\mathbf{r}) \Phi(\mathbf{r}) \rangle. \end{aligned} \quad (2.2)$$

This constraint has already been taken into account in Eq. (2.1), with the Fermi chemical potential μ and Bose chemical potential $\mu_M \equiv 2\mu[1]$. $V_{\text{trap}}^F(\mathbf{r})$ and $V_{\text{trap}}^M(\mathbf{r})$ are the harmonic trap potentials for Fermi atoms and Bose molecules, respectively, which are assumed to be isotropic

$$V_{\text{trap}}^F = \frac{1}{2} m \omega_0^2 r^2, \quad V_{\text{trap}}^M = \frac{1}{2} M \omega_{0M}^2 r^2. \quad (2.3)$$

In addition, in this paper, we assume that the atoms and molecules feel the same trap frequency $\omega_0 = \omega_{0M}$ (which correctly describes recent experiments).

To study the BCS-BEC crossover phenomenon, we extend the theory at $T = 0$ developed by Leggett[9] in the context of superconductivity to include a Feshbach resonance as well as the effect of a harmonic trap potential. The key point of this theory is to solve the mean-field gap equation for the order parameter together with the equation for the number of particles, which determines the Fermi chemical potential μ . In the BCS-BEC crossover, μ decreases from the usual BCS limit given by the Fermi energy ε_F and can become negative. The *thermal* fluctuations in the Cooper-channel and the *thermal* excitations of Bose condensate fluctuations, crucial in considering the BEC-BEC crossover at finite temperatures close to T_c [1, 2, 3, 4, 10, 12, 13, 14, 15], are not important at $T = 0$. Such fluctuations will not be considered in the present paper.

The gap equation is obtained from the mean-field approximation for Eq. (2.1) in terms of the BCS Cooper-pair condensate $\Delta(\mathbf{r}) \equiv U \langle \Psi_{\downarrow}(\mathbf{r}) \Psi_{\uparrow}(\mathbf{r}) \rangle$ as well as the molecular BEC condensate $\phi_M(\mathbf{r}) \equiv \langle \Phi(\mathbf{r}) \rangle$. The Hartree-Fock-Bogoliubov (HFB) mean-field Hamiltonian for the *fermions* is given by

$$H_{\text{HFB}} = \sum_{\sigma} \int d\mathbf{r} \hat{\Psi}_{\sigma}^{\dagger}(\mathbf{r}) \left[-\frac{\nabla^2}{2m} - \frac{U}{2} n_F(\mathbf{r}) + V_{\text{trap}}^F(r) - \mu \right] \Psi_{\sigma}(\mathbf{r})$$

$$\begin{aligned}
& - \int d\mathbf{r} \Delta(\mathbf{r}) [\hat{\Psi}_\uparrow^\dagger(\mathbf{r}) \hat{\Psi}_\downarrow^\dagger(\mathbf{r}) + h.c.] + g_r \int d\mathbf{r} \phi_M(\mathbf{r}) [\hat{\Psi}_\uparrow^\dagger(\mathbf{r}) \hat{\Psi}_\downarrow^\dagger(\mathbf{r}) + h.c.] \\
& = \sum_\sigma \int d\mathbf{r} \hat{\Psi}_\sigma^\dagger(\mathbf{r}) \left[-\frac{\nabla^2}{2m} - \frac{U}{2} n_F(\mathbf{r}) + V_{\text{trap}}^F(r) - \mu \right] \Psi_\sigma(\mathbf{r}) \\
& - \int d\mathbf{r} \tilde{\Delta}(\mathbf{r}) [\hat{\Psi}_\uparrow^\dagger(\mathbf{r}) \hat{\Psi}_\downarrow^\dagger(\mathbf{r}) + h.c.]. \tag{2.4}
\end{aligned}$$

In Eq. (2.4), the Cooper-pair order parameter $\Delta(\mathbf{r})$ and the molecular condensate $\phi_M(\mathbf{r})$ are taken to be real, without loss of generality. $n_F(\mathbf{r}) \equiv \sum_\sigma \langle \Psi_\sigma^\dagger(\mathbf{r}) \Psi_\sigma(\mathbf{r}) \rangle$ is the local number density of Fermi atoms. Equation (2.4) clearly has the same form as the usual BCS-Gor'kov Hamiltonian, but now with the Cooper-pair order parameter $\Delta(\mathbf{r})$ replaced with the *composite* order parameter,

$$\tilde{\Delta}(\mathbf{r}) \equiv \Delta(\mathbf{r}) - g_r \phi_M(\mathbf{r}). \tag{2.5}$$

Because of the spherical symmetry of our harmonic trap, $\Delta(\mathbf{r})$, $\phi_M(\mathbf{r})$, $\tilde{\Delta}(\mathbf{r})$, and $n_F(\mathbf{r})$ only depend on $|\mathbf{r}|$.

Since we are only discussing $T = 0$ in this paper, the molecules described by $\Phi(\mathbf{r})$ are all Bose-condensed. As noted above, we ignore excitations of this molecular condensate. Thus the HFB mean-field Hamiltonian in Eq. (2.4) does not involve the dynamics of the molecular condensate. The latter only enters through the equilibrium value $\tilde{\Delta}(\mathbf{r})$.

Superfluidity in our coupled fermion-boson model is characterized by the two broken-symmetry order parameters, i.e., the BCS order parameter $\Delta(\mathbf{r}) = U \langle \Psi_\downarrow(\mathbf{r}) \Psi_\uparrow(\mathbf{r}) \rangle$ and the molecular BEC condensate $\phi_M(\mathbf{r}) = \langle \Phi(\mathbf{r}) \rangle$. However, these are strongly coupled to each other and hence are not independent. One finds from Eq. (2.1) that their equilibrium values satisfy

$$\frac{g_r}{U} \Delta(\mathbf{r}) + \left[-\frac{\nabla^2}{2M} + V_{\text{trap}}^M(r) + 2\nu - 2\mu \right] \phi_M(\mathbf{r}) = 0. \tag{2.6}$$

This is in fact an exact identity, and can be obtained from the equation of motion

$$0 = \frac{d\phi_M(\mathbf{r}, t)}{dt} = \frac{i}{\hbar} \langle [H, \Phi(\mathbf{r}, t)] \rangle. \tag{2.7}$$

In the absence of a trap, Eq. (2.6) reduces to

$$\frac{g_r}{U} \Delta + (2\nu - 2\mu) \phi_M = 0, \tag{2.8}$$

a result discussed at length in Refs. [1, 3]. As a result of this strong coupling, the Cooper-pair and Feshbach molecule condensates are hybridized by the Feshbach resonance, and are both finite throughout the superfluid phase.

In a uniform gas, the composite order parameter appearing in Eq. (2.4) and defined in Eq. (2.5) can be written in the form

$$\tilde{\Delta} = U_{\text{eff}} \sum_{\mathbf{p}} \langle c_{-\mathbf{p}\downarrow} c_{\mathbf{p}\uparrow} \rangle, \quad (2.9)$$

where $c_{\mathbf{p}\sigma}$ the annihilation operator of a Fermi atom in momentum space, and[1, 3]

$$U_{\text{eff}} \equiv U + \frac{g_r^2}{2\nu - 2\mu}. \quad (2.10)$$

U_{eff} describes an effective pairing interaction in a BCS-type Hamiltonian in Eq. (2.4), which can be tuned by adjusting the molecular threshold energy 2ν . We note that the expression in Eq. (2.9) has the same form as the usual definition of a BCS Cooper-pair, apart from the effective pairing interaction U_{eff} .

The molecular Bose excitations are described by the field operator $\delta\Phi(\mathbf{r}) \equiv \Phi(\mathbf{r}) - \langle \Phi(\mathbf{r}) \rangle = \Phi(\mathbf{r}) - \phi_m(\mathbf{r})$. When we substitute this expression into the boson kinetic term [the bilinear term involving $\Phi(\mathbf{r})$] in Eq. (2.1), the terms linear in $\delta\Phi(\mathbf{r})$ are cancelled out by another term which is linear in $\delta\Phi(\mathbf{r})$ arising from the last term in Eq. (2.1). This is a consequence of the key relation in Eq. (2.6). This leaves a term in Eq. (2.1) which is bilinear in $\delta\Phi(\mathbf{r})$, namely

$$H_M = \int d\mathbf{r} \delta\Phi^\dagger(\mathbf{r}) \left[-\frac{\nabla^2}{2M} + 2\nu + V_{\text{trap}}^M(r) - 2\mu \right] \delta\Phi(\mathbf{r}). \quad (2.11)$$

Equation (2.11) gives the lowest molecular excitation energy $E_0^M \equiv 2\nu + (3/2)\omega_0 - 2\mu$. A self-consistent calculation shows that this threshold energy is always *positive* (i.e., $2\nu + (3/2)\hbar\omega_0 > 2\mu$). As discussed in Ref. [3] for the uniform case, this contradicts the fact that excitation spectrum must be *gapless* in a uniform interacting Bose gas (of molecules). Although Eq. (2.1) does not explicitly involve an interaction between the molecules, an effective repulsive interaction is induced by the Fermi gas[3, 33, 34]. This effective repulsive interaction will lead to a Bogoliubov phonon as the collective mode in the molecular gas in the BEC regime.

In an interacting Bose gas, it is well known that the only low-energy excitations are collective modes. This is because the single-particle excitations are strongly hybridized[35] with the two-particle excitations (including collective modes). When we include the effective molecule-molecule interaction in a consistent way, the gapless or phonon behavior of molecular Bose excitations in a uniform gas must be recovered. This requires an extended

version of the present theory, as we shall discuss in a future paper[36]. The present paper is mainly concerned with the single-particle excitations of a Fermi superfluid, and does not deal with the collective modes. The fact that our present treatment does not include the correct interaction[33, 34] between molecules in the BEC limit is of little importance when discussing the spectrum of the single-particle Fermi excitations (which disappear as we approach the BEC limit).

The mean-field HFB Hamiltonian in Eq. (2.4) is formally identical to a trapped superfluid Fermi gas in the standard BCS treatment, apart from the replacement of $\Delta(\mathbf{r})$ by the (self-consistent) composite order parameter $\tilde{\Delta}(\mathbf{r})$. Bruun and co-workers have presented detailed numerical results for the Cooper pair order parameter and the single-particle BCS excitations in a BCS superfluid at $T = 0$ [37, 38, 39, 40]. Our present work may be viewed as a natural extension to include the effect of the Feshbach resonance, based on the model in Eq. (2.4) involving the effective pair potential $\tilde{\Delta}(\mathbf{r})$. The latter, of course, involves the molecular condensate $\phi_M(\mathbf{r})$ and must be computed self-consistently.

As usual, the HFB Hamiltonian in Eq. (2.4) can be diagonalized as $H_{\text{HFB}} = \sum_{n\sigma} E_n \gamma_{n\sigma}^\dagger \gamma_{n\sigma}$ by solving the Bogoliubov de Gennes (BdG) equations[41],

$$\begin{pmatrix} H_0 & \tilde{\Delta}(\mathbf{r}) \\ \tilde{\Delta}(\mathbf{r}) & -H_0 \end{pmatrix} \begin{pmatrix} u_n(\mathbf{r}) \\ v_n(\mathbf{r}) \end{pmatrix} = E_n \begin{pmatrix} u_n(\mathbf{r}) \\ v_n(\mathbf{r}) \end{pmatrix}, \quad (2.12)$$

where H_0 is the diagonal component of H_{HFB} . The Bogoliubov quasiparticle excitations are described by the fermion operators $\gamma_{n\sigma}$, which are related to the fermion field operator $\Psi_\sigma(\mathbf{r})$ as[41]

$$\begin{aligned} \Psi_\uparrow(\mathbf{r}) &= \sum_n \left[u_n(\mathbf{r}) \gamma_{n\uparrow} + v_n^*(\mathbf{r}) \gamma_{n\downarrow}^\dagger \right], \\ \Psi_\downarrow(\mathbf{r}) &= \sum_n \left[u_n(\mathbf{r}) \gamma_{n\downarrow} - v_n^*(\mathbf{r}) \gamma_{n\uparrow}^\dagger \right]. \end{aligned} \quad (2.13)$$

As noted above, the solutions of these BdG equations for a trapped Fermi gas have been discussed extensively by Bruun and co-workers[37, 38, 39, 40] in the BCS limit and where $\tilde{\Delta}(\mathbf{r}) = \Delta(\mathbf{r})$. It is convenient to expand the fermion field operator $\Psi_\sigma(\mathbf{r})$ with respect to the eigenfunctions of a harmonic potential $V_{\text{trap}}^F(r)$ as

$$\hat{\Psi}_\sigma(\mathbf{r}) = \sum_{nlm} f_{nlm}^F(\mathbf{r}) c_{nlm\sigma}. \quad (2.14)$$

Here, $f_{nlm}^F(\mathbf{r}) \equiv R_{nl}^F(r) Y_{lm}(\hat{\theta})$, where $Y_{lm}(\hat{\theta})$ is a spherical harmonic and $R_{nl}^F(r)$ is the usual

radial wavefunction, given by

$$R_{nl}^F(r) = \sqrt{2}(m\omega_0)^{3/4} \sqrt{\frac{n!}{(n+l+1/2)!}} e^{-\frac{\bar{r}^2}{2}} \bar{r}^l L_n^{l+1/2}(\bar{r}^2) \quad (\bar{r} \equiv \sqrt{m\omega_0}r), \quad (2.15)$$

where $L_n^{l+1/2}(\bar{r}^2)$ is a Laguerre polynomial. The HFB Hamiltonian H_{HFB} in Eq. (2.4) can then be reduced to

$$H_{\text{HFB}} = \sum_{nlm,\sigma} \xi_{nl}^F c_{nlm\sigma}^\dagger c_{nlm\sigma} - \frac{U}{2} \sum_{nn'lm,\sigma} J_{nn'}^l c_{nlm\sigma}^\dagger c_{n'l\sigma} - \sum_{nn'lm} F_{nn'}^l [c_{nlm\uparrow}^\dagger c_{n'l,-m\downarrow}^\dagger + h.c.]. \quad (2.16)$$

Here $\xi_{nl}^F = \hbar\omega_0(2n+l+3/2) - \mu$ are the single-particle excitation energies of the atoms in the harmonic potential. $F_{nn'}^l$ and $J_{nn'}^l$ describe the mean field effects associated with the composite pair potential $\tilde{\Delta}(r)$ (which plays the role of an ‘‘off-diagonal’’ potential) and the Hartree potential $-\frac{U}{2}n_F(r)$, respectively. These are given by

$$F_{nn'}^l \equiv \int_0^\infty r^2 dr R_{nl}^F(r) \tilde{\Delta}(r) R_{n'l}^F(r), \quad (2.17)$$

$$J_{nn'}^l \equiv \int_0^\infty r^2 dr R_{nl}^F(r) n_F(r) R_{n'l}^F(r). \quad (2.18)$$

We note that $F_{nn'}^l$ and $J_{nn'}^l$ include both the intra-shell terms ($n = n'$) as well as the inter-shell terms ($n \neq n'$). The local Cooper-pair order parameter and fermion density are given by[37]

$$\Delta(r) = U \sum_{nn'l} \frac{2l+1}{4\pi} R_{nl}^F(r) R_{n'l}^F(r) \langle c_{nl0\downarrow} c_{n'l0\uparrow} \rangle, \quad (2.19)$$

$$n_F(r) = \sum_{nn'l\sigma} \frac{2l+1}{4\pi} R_{nl}^F(r) R_{n'l}^F(r) \langle c_{nl0\sigma}^\dagger c_{n'l0\sigma} \rangle. \quad (2.20)$$

In Eq. (2.20), we have taken advantage of the spherical symmetry of our model, which leads to $\langle c_{nlm\downarrow} c_{n'l,-m\uparrow} \rangle = \langle c_{nl0\downarrow} c_{n'l0\uparrow} \rangle$ and $\langle c_{nlm\sigma}^\dagger c_{n'lm\sigma} \rangle = \langle c_{nl0\sigma}^\dagger c_{n'l0\sigma} \rangle$.

It is important to remember that Eq. (2.16) includes the effect of the molecular condensate $\phi_M(r)$, since it enters the composite order parameter $\tilde{\Delta}(r) = \Delta(r) - g_r \phi_M(r)$. Since $\phi_M(r)$ only depends on r , we need only consider the $l = 0$ quantum number. Thus we can expand $\phi_M(r)$ in terms of the radial components

$$\phi_M(r) = \frac{1}{\sqrt{4\pi}} \sum_n \alpha_n R_{n0}^M(r). \quad (2.21)$$

Here $f_{nlm}^M(\mathbf{r}) \equiv R_{nl}^M(r)Y_{lm}(\hat{\theta})$ is a molecular eigenfunction for the isotropic harmonic potential $V_{\text{trap}}^M(r)$, with the molecular energy $E_{nl}^M = \hbar\omega_0(2n + l + 3/2)$. The radial component $R_{nl}^M(r)$ is identical to that given in Eq. (2.15), except that the atom mass m is now replaced by the bound state mass $M = 2m$. Substituting Eq. (2.21) into Eq. (2.6), we obtain an expression for α_n in terms of $\Delta(r)$,

$$\alpha_n = -\frac{g_r}{U} \frac{\sqrt{4\pi}}{E_{n0}^M + 2\nu - 2\mu} \int_0^\infty dr r^2 \Delta(r) R_{n0}^M(r). \quad (2.22)$$

The magnitude of the various expansion coefficients α_n clearly determines to what extent the molecular condensate $\phi_M(r)$ in Eq. (2.21) is similar to the BEC order parameter $\phi_M^{\text{ideal}}(r)$ of a non-interacting Bose gas of molecules in a harmonic trap. The latter is given by the macroscopic occupation of the lowest ($n = 0$) state

$$\phi_M^{\text{ideal}}(r) = \frac{1}{\sqrt{4\pi}} \alpha_0 R_{00}^M(r), \quad (2.23)$$

where $|\alpha_0| = \sqrt{N/2}$ for a non-interacting Bose gas.

Since Eq. (2.16) can be written as $H_{\text{HFB}} = \sum_{ml} H_{\text{HFB}}^{ml}$, one may independently diagonalize each H_{HFB}^{ml} , i.e., for each set of values (l, m), by a unitary transformation. This is the Bogoliubov transformation,

$$\begin{pmatrix} c_{0lm\uparrow} \\ \dots \\ c_{N_l lm\uparrow} \\ c_{0l, -m\downarrow}^\dagger \\ \dots \\ c_{N_l l, -m\downarrow}^\dagger \end{pmatrix} = \hat{W}^l \begin{pmatrix} \gamma_{0lm\uparrow} \\ \dots \\ \gamma_{N_l lm\uparrow} \\ \gamma_{0lm\downarrow}^\dagger \\ \dots \\ \gamma_{N_l lm\downarrow}^\dagger \end{pmatrix}. \quad (2.24)$$

Here \hat{W}^l is a $2(N_l + 1) \times 2(N_l + 1)$ -orthogonal matrix, and the fermion operator $\gamma_{nlm\sigma}$ describes the Bogoliubov quasi-particles. Physically, the matrix elements of \hat{W}^l describe the hybridization of particle and hole excitations in the Bogoliubov quasi-particles described by $\gamma_{nlm\sigma}$. \hat{W}^l is determined by the requirement that $\hat{W}^{l\dagger} H_{\text{HFB}}^{ml} \hat{W}^l$ be diagonal. The matrix elements W_{ij}^l are then obtained from the eigenfunctions of the following BdG equations for

H_{HFB}^{ml} [42],

$$\begin{pmatrix}
\xi_{0l}^F - \frac{U}{2} J_{00}^l & \cdots & -\frac{U}{2} J_{0N_l}^l & -F_{00}^l & \cdots & -F_{0N_l}^l \\
\cdots & \cdots & \cdots & \cdots & \cdots & \cdots \\
-\frac{U}{2} J_{N_l 0}^l & \cdots & \xi_{N_l l}^F - \frac{U}{2} J_{N_l N_l}^l & -F_{N_l 0}^l & \cdots & -F_{N_l N_l}^l \\
-F_{00}^l & \cdots & -F_{0N_l}^l & -\xi_{0l}^F + \frac{U}{2} J_{00}^l & \cdots & \frac{U}{2} J_{0N_l}^l \\
\cdots & \cdots & \cdots & \cdots & \cdots & \cdots \\
-F_{N_l 0}^l & \cdots & -F_{N_l N_l}^l & \frac{U}{2} J_{N_l 0}^l & \cdots & -\xi_{N_l l}^F + \frac{U}{2} J_{N_l N_l}^l
\end{pmatrix}
\begin{pmatrix}
W_{0,n}^l \\
\cdots \\
W_{N_l,n}^l \\
W_{N_l+1,n}^l \\
\cdots \\
W_{2N_l+2,n}^l
\end{pmatrix}
= E_{nl}^F
\begin{pmatrix}
W_{0,n}^l \\
\cdots \\
W_{N_l,n}^l \\
W_{N_l+1,n}^l \\
\cdots \\
W_{2N_l+2,n}^l
\end{pmatrix} \quad (2.25)$$

As usual, we introduce a cutoff $\omega_c \equiv \hbar\omega_0(N_c + 3/2)$ in the energy summation in the gap equation [see Eq. (2.27) below]. This defines N_c . The maximal radial quantum number N_l in Eq. (2.25) is then given by the largest integer bounded by $(N_c - l)/2$. As with the usual BdG equations, positive and negative eigenenergies (E_{nl}^F and $-E_{nl}^F$) are obtained from Eq. (2.25). The diagonalized Hamiltonian can be written using only the positive energy eigenenergies ($E_{nl}^F \geq 0$), namely

$$\begin{aligned}
H_{\text{HFB}}^F &= \sum_{n=0}^{N_l} \left[E_{nl}^F \gamma_{nlm\uparrow}^\dagger \gamma_{nlm\uparrow} - E_{nl}^F \gamma_{nlm\downarrow}^\dagger \gamma_{nlm\downarrow} \right] \\
&= \sum_{n=0}^{N_l} E_{nl}^F + \sum_{n=0,\sigma}^{N_l} E_{nl}^F \gamma_{nlm\sigma}^\dagger \gamma_{nlm\sigma}. \quad (2.26)
\end{aligned}$$

In the following discussion, we only take the *positive* eigenenergies E_{nl}^F as in Eq. (2.26). According to Eq. (2.26), the operator $\gamma_{nlm\sigma}^\dagger$ describes creating a Fermi single-particle excitation from the ground state, with excitation energy $E_{nl}^F \geq 0$. Because of the assumed spherical symmetry of our trap, E_{nl}^F and \hat{W}^l do not depend on the quantum number m . Substituting Eq. (2.24) into Eqs. (2.19) and (2.20), we obtain (at $T = 0$)

$$\Delta(r) = U \sum_{nn'l} \frac{2l+1}{4\pi} R_{nl}^F(r) R_{n'l}^F(r) \sum_{j=0}^{N_l} W_{\bar{N}_l+n, \bar{N}_l+j}^l W_{n'+1, \bar{N}_l+j}^l, \quad (2.27)$$

$$n_{\text{F}}(r) = \sum_{nn'l} \frac{2l+1}{4\pi} R_{nl}^F(r) R_{n'l}^F(r) \sum_{j=0}^{N_l} \left[W_{n+1, \bar{N}_l+j}^l W_{n'+1, \bar{N}_l+j}^l + W_{\bar{N}_l+n, j+1}^l W_{\bar{N}_l+n', j+1}^l \right], \quad (2.28)$$

where $\bar{N}_l \equiv N_l + 2$ and the prime in \sum' refers to the finite cutoff ω_c in the summation (see above).

In the BCS-BEC crossover region, we shall find that the Fermi chemical potential μ deviates strongly from the usual BCS limit, where it equals the Fermi energy ε_F . This effect is taken into account by considering the equation for the number of atoms in addition to the BdG equations[9]. Since non-condensed molecules are absent at $T = 0$, the *total* number density of Fermi atoms $n(r)$ is simply given by

$$n(r) = 2|\phi_M(r)|^2 + n_F(r) \equiv 2n_M(r) + n_F(r), \quad (2.29)$$

where each molecule counts for two Fermi atoms. The equation for the total number of atoms, which determines μ , is then obtained by integrating Eq. (2.29) over \mathbf{r} . The result is

$$\begin{aligned} N &= 2 \sum_n \alpha_n^2 + \sum_{nn'l} (2l+1) \left[|W_{n+1, \bar{N}_l+n'}^l|^2 + |W_{\bar{N}_l+n, n'+1}^l|^2 \right] \\ &\equiv 2N_M + N_F. \end{aligned} \quad (2.30)$$

Here N_M and N_F are the number of (Feshbach) molecular bosons and number of Fermi atoms in the crossover region, respectively. Equations (2.25) and Eq. (2.30) are the basic equations of our theory at $T = 0$, taking into account a Bose condensate of Cooper-pairs and molecules in a self-consistent manner. We numerically solve the BdG equations (2.25) together with the generalized number equation in Eq. (2.30), determining the coefficient α_n [see Eq. (2.22)], $\Delta(r)$, $\phi_M(r)$, $n_F(r)$ and μ self-consistently.

In order to understand the essential physics, we end this Section by recalling what the above formalism reduces to for a *uniform* superfluid Fermi gas. In this case, the simple pairing mean-field approximation (MFA) gives usual BCS-Gor'kov expressions for the diagonal and off-diagonal single-particle Green's functions

$$G_{11}(\mathbf{p}, \omega) = \frac{\omega + \xi_{\mathbf{p}}}{\omega^2 - E_{\mathbf{p}}^2}, \quad G_{12}(\mathbf{p}, \omega) = -\frac{\tilde{\Delta}}{\omega^2 - E_{\mathbf{p}}^2}, \quad (2.31)$$

with the BCS-Bogoliubov excitation energy given by

$$E_{\mathbf{p}} = \sqrt{(\varepsilon_{\mathbf{p}} - \mu)^2 + |\tilde{\Delta}|^2}. \quad (2.32)$$

Here $\xi_{\mathbf{p}} \equiv \varepsilon_{\mathbf{p}} - \mu$ (where $\varepsilon_{\mathbf{p}} = p^2/2m$) is the kinetic energy measured from the chemical potential. Using $G_{12}(\mathbf{p}, \omega)$ to calculate Δ , one finds that $\tilde{\Delta}$ in Eq. (2.9) satisfies the usual

“gap equation” [but now with the pairing interaction U_{eff} given by Eq. (2.10)],

$$\tilde{\Delta} = U_{\text{eff}} \sum_{\mathbf{p}}' \frac{\tilde{\Delta}}{2E_{\mathbf{p}}} \tanh \frac{1}{2}\beta E_{\mathbf{p}}, \quad (2.33)$$

valid at finite temperatures. As usual, a cutoff is introduced in the momentum summation. At this MFA level, the total number of atoms at $T = 0$ has the same form as Eq. (2.30),

$$N = 2N_M + N_F. \quad (2.34)$$

The number of Fermi atoms in Eq. (2.34) is now given [using $G_{11}(\mathbf{p}, \omega)$] by the well-known BCS expression

$$N_F = \sum_{\mathbf{p}, \sigma} \langle c_{\mathbf{p}\sigma}^\dagger c_{\mathbf{p}\sigma} \rangle = \sum_{\mathbf{p}} \left[1 - \frac{\xi_{\mathbf{p}}}{E_{\mathbf{p}}} \tanh \frac{1}{2}\beta E_{\mathbf{p}} \right], \quad (2.35)$$

while the number of condensed molecules is $N_M = |\phi_M|^2$.

In the uniform gas, the values of μ and $\tilde{\Delta}$ are determined by the self-consistent solutions of the MFA gap equation (2.33) and the number equation given by Eqs. (2.34). This simple “pairing approximation” for the single-particle Fermi excitations is expected to give a quantitative description at $T = 0$ [where $\tanh \frac{1}{2}\beta E_{\mathbf{p}} \rightarrow 1$ in Eqs. (2.33) and (2.35)], since fluctuations are small and all the molecules are Bose-condensed. This $T = 0$ limit was first studied by Eagles[8] and Leggett[9] in the absence of a Feshbach resonance. As we mentioned earlier, for T approaching T_c , the fluctuations associated with exciting molecules out of the condensate and coupling to the particle-particle (Cooper-pair) channel become dominant.

These fluctuations (rather than the breaking up of two-particle bound states) were first included by Nozières and Schmitt-Rink (NSR)[10] to determine T_c . In Ref. [3], we extended this NSR approach to discuss the superfluid phase *below* T_c in a *uniform* Fermi gas, including a Feshbach resonance and associated molecular bosons. Both $\tilde{\Delta}$ and μ are obtained by solving Eqs. (2.33) and (2.34) self-consistently, but now include the depletion of $\tilde{\Delta}$ through the presence of non-Bose-condensed molecules. This procedure gives the simplest extension of the MFA-BCS single-particle results, in that now Eqs. (2.31) and (2.32) involve values of μ and $\tilde{\Delta}$ which include (in an average way) the effect of fluctuations around the MFA theory. The effect of such fluctuations is of considerable current interest[43, 44] and lead to what is called the “pseudogap” regime (for a recent review, see Ref. [45]). In this region, strong low-energy fluctuations in the Cooper-channel suppress the density of states around the Fermi energy, which has the same effect as if there was an effective pair potential, even

outside the superfluid region ($T > T_c$) where $\tilde{\Delta}(r)$ vanishes. In a future paper, we will use this generalized NSR approach to include fluctuations and extend the results of the present paper to finite temperatures.

III. SINGLE-PARTICLE GREEN'S FUNCTIONS

In ordinary BCS superfluidity, the single-particle excitations (BCS quasiparticles) are associated with dissociation of weakly-bound Cooper-pairs. In the coupled fermion-boson model in Eq. (2.4), these Cooper pairs are replaced by composite bosons, consisting of Cooper-pairs and molecular bosons associated with the Feshbach resonance [$\tilde{\Delta}(\mathbf{r}) \equiv \Delta(\mathbf{r}) - g_r\phi_M(\mathbf{r})$]. Even in the BEC regime ($2\nu < 0$), Fermi excitations can still exist[30] as well as collective modes (which form a Bose spectrum). As more and more fermions pair up to form bosons, the spectral weight of the Fermi branch vanishes, shifting to the Bose collective branch.

Single-particle properties are most conveniently discussed in terms of Green's functions. The "diagonal" single-particle thermal Green's function $G_{11}(\mathbf{r}, \mathbf{r}', i\omega_m)$ is defined by[46, 47, 48]

$$G_{11}(\mathbf{r}, \mathbf{r}', i\omega_m) = - \int_0^\beta d\tau e^{i\omega_m\tau} \langle T_\tau \{ \Psi_\uparrow(\mathbf{r}, \tau) \Psi_\uparrow^\dagger(\mathbf{r}', 0) \} \rangle, \quad (3.1)$$

where $i\omega_m$ is the fermion Matsubara frequency associated with the imaginary time τ . One needs three other single-particle Green's functions to describe a Fermi superfluid, as summarized by the 2×2 matrix Green's function[47]

$$\begin{aligned} \hat{G}(\mathbf{r}, \mathbf{r}', i\omega_m) &= \begin{pmatrix} G_{11}(\mathbf{r}, \mathbf{r}', i\omega_m) & G_{12}(\mathbf{r}, \mathbf{r}', i\omega_m) \\ G_{21}(\mathbf{r}, \mathbf{r}', i\omega_m) & G_{22}(\mathbf{r}, \mathbf{r}', i\omega_m) \end{pmatrix} \\ &= - \int_0^\beta d\tau e^{i\omega_m\tau} \begin{pmatrix} \langle T_\tau \{ \Psi_\uparrow(\mathbf{r}, \tau) \Psi_\uparrow^\dagger(\mathbf{r}', 0) \} \rangle, & \langle T_\tau \{ \Psi_\uparrow(\mathbf{r}, \tau) \Psi_\downarrow(\mathbf{r}', 0) \} \rangle \\ \langle T_\tau \{ \Psi_\downarrow^\dagger(\mathbf{r}, \tau) \Psi_\uparrow^\dagger(\mathbf{r}', 0) \} \rangle, & \langle T_\tau \{ \Psi_\downarrow^\dagger(\mathbf{r}, \tau) \Psi_\downarrow(\mathbf{r}', 0) \} \rangle \end{pmatrix}. \end{aligned} \quad (3.2)$$

In Eq. (3.2), G_{22} gives the single-particle excitation spectrum of Fermi atoms of pseudospin \downarrow . The off-diagonal components G_{12} and G_{21} arise as a direct consequence of the broken symmetry and the presence of a condensate of Cooper pairs. Using the BdG equations in Eq. (2.12), one can show that these Green's functions are related to each other as $G_{22}(\mathbf{r}', \mathbf{r}, i\omega_m) = -G_{11}(\mathbf{r}, \mathbf{r}', i\omega_m)$, and $G_{21}^*(\mathbf{r}', \mathbf{r}, -i\omega_m) = G_{12}(\mathbf{r}, \mathbf{r}', i\omega_m)$. From the definition

of the Cooper-pair order parameter $\Delta(r) = U\langle\Psi_{\downarrow}(\mathbf{r})\Psi_{\uparrow}(\mathbf{r})\rangle$, we find the important self-consistency condition (the gap equation)

$$\Delta(r) = \frac{1}{\beta} \sum'_{\omega_m} G_{12}(\mathbf{r}, \mathbf{r}, i\omega_m). \quad (3.3)$$

Using the eigenfunctions $f_{lmn}^F(\mathbf{r})$ defined in Eq. (2.14), we can write 2×2 single-particle Green's function in Eq. (3.2) as

$$\hat{G}(\mathbf{r}, \mathbf{r}', i\omega_m) = \sum_{lm} Y_{lm}(\hat{\theta}) \hat{g}^l(r, r', i\omega_m) Y_{lm}^*(\hat{\theta}'), \quad (3.4)$$

where $\hat{g}^l(r, r', i\omega_m)$ is the 2×2 Green's function for a given value of the angular momentum l ,

$$\hat{g}^l(r, r', i\omega_m) = \sum_{j=0}^{N_l} \left[\frac{\Lambda_{jl}(r) \Lambda_{jl}^\dagger(r')}{i\omega_m - E_{jl}^F} + \frac{\bar{\Lambda}_{jl}(r) \bar{\Lambda}_{jl}^\dagger(r')}{i\omega_m + E_{jl}^F} \right]. \quad (3.5)$$

The two-component spinor $\Lambda_{jl}(r)$ in Eq. (3.5) is defined in terms of the solutions of the BdG equations in Eq. (2.25), namely

$$\Lambda_{jl}(r) = \sum_{n=0}^{N_l} \begin{pmatrix} W_{n+1, j+1}^l \\ W_{N_l+n, j+1}^l \end{pmatrix} R_{nl}^F(r), \quad \bar{\Lambda}_{jl}(r) = i\tau_2 \Lambda_{jl}(r). \quad (3.6)$$

Here τ_2 is the Pauli matrix.

A very useful quantity is the Fermi single-particle excitation spectrum $N(\omega)$, also referred to as the density-of-states (DOS). This is related to the spectrum of single-particle Green's function,

$$N(\omega) = -\frac{1}{\pi} \int d\mathbf{r} \text{Im} [G_{11}(\mathbf{r}, \mathbf{r}, i\omega_m \rightarrow \omega + i\delta)]. \quad (3.7)$$

Substituting Eqs. (3.4) and (3.5) into Eq. (3.7), this *spatially-averaged* density-of-states (per pseudospin) is given by ($E_{jl}^F > 0$)

$$N(\omega) = \sum_l (2l+1) \sum_{n,j} |W_{n+1, j+1}^l|^2 \delta(\omega - E_{jl}^F) \quad (\omega \geq 0). \quad (3.8)$$

It is also useful to introduce the *local* density of states (LDOS), defined as

$$\begin{aligned} N(\omega, r) &\equiv -\frac{1}{\pi} \text{Im} [G_{11}(\mathbf{r}, \mathbf{r}, i\omega_m \rightarrow \omega + i\delta)] \\ &= \sum_{mn'l} \frac{2l+1}{4\pi} R_{nl}^F(r) R_{n'l}^F(r) \sum_j W_{n+1, j+1}^l W_{n'+1, j+1}^l \delta(\omega - E_{jl}^F). \end{aligned} \quad (3.9)$$

The local density of states LDOS in Eq. (3.9) is simply related to the spatially-averaged total DOS in Eq. (3.8) by

$$N(\omega) \equiv \int_0^\infty 4\pi r^2 dr N(\omega, r). \quad (3.10)$$

The gap equation (2.27) is easily obtained from the present Green's function formalism. When we use the off-diagonal (1,2)-component of Eq. (3.5) in Eq. (3.3), we obtain

$$\Delta(r) = -U \sum_{nn'l} \frac{2l+1}{4\pi} R_{nl}^F(r) R_{n'l}^F(r) \sum_{j=0}^{N_l} W_{\bar{N}_l+n, j+1}^l W_{n'+1, j+1}^l. \quad (3.11)$$

Once one has $\Delta(r)$, one can calculate the coefficients α_n in Eq. (2.22) and then find $\phi_M(r)$. By this procedure, one finally obtains the value of $\tilde{\Delta}(r)$, with the total number equation in Eq. (2.30) determining the self-consistent values. As with the usual BdG equations in a uniform BCS model, there is a relation between eigenfunctions for $E_{nl}^F \geq 0$ and $E_{nl}^F \leq 0$, which is given by[41]

$$\sum_n \begin{pmatrix} W_{\bar{N}_l+n, j+1}^l \\ -W_{n+1, j+1}^l \end{pmatrix} R_{nl}^F(r) = \sum_n \begin{pmatrix} W_{n+1, \bar{N}_l+j}^l \\ W_{\bar{N}_l+n, \bar{N}_l+j}^l \end{pmatrix} R_{nl}^F(r). \quad (3.12)$$

Substituting Eq. (3.12) into Eq. (3.11), we find that the gap equation (2.27) for the Cooper-pair order parameter $\Delta(r)$ is reproduced.

IV. SCATTERING LENGTHS, GAP EQUATION AND STRENGTH OF FESHBACH RESONANCES

The Hamiltonian in Eq. (2.1) involves the bare energies U , g_r and 2ν . As usual in dealing with ultracold atomic gases, it is convenient to work in terms of renormalized interaction energies which incorporate the effect of high energy processes. This procedure naturally leads to the two-body scattering length a_s^{2b} which describes the effective interaction between low energy atoms, even in the case of a Feshbach resonance. The two-body scattering length a_s^{2b} can be measured directly in a variety of ways.

In this section, we briefly review the standard theory for renormalized low energy parameters (see, for example, Sec. IV A of Ref. [2] and Refs. [4, 7, 12]). We also point out that in the presence of a Feshbach resonance, the self-consistent gap equation which determines the order parameter naturally introduce a *different* s -wave scattering length a_s , which has a crucial dependence on the Fermi chemical potential μ . As a result, in dealing with the

BCS-BEC crossover in Fermi superfluids, it seems most natural to treat a_s as the control parameter, rather than a_s^{2b} .

There is a second reason which makes it useful to discuss properties in crossover region as a function of a_s . Before doing so, we discuss the parameters we use in this paper. We take the total number of atoms to be $N = 10,912$ ($= N_\uparrow + N_\downarrow = 2N_\uparrow$). In a non-interacting Fermi gas, this corresponds to filling atoms (per spin) up to $E = 31.5\hbar\omega_0$ ($\equiv \varepsilon_F$), where ω_0 is the trap frequency. As the unit of length, we use the Thomas-Fermi radius $R_F \equiv \sqrt{2\varepsilon_F/m\omega_0^2}$ for a free Fermi gas in the trap. We take the Feshbach coupling constant $g_r = 0.06\omega_0$ ($\bar{g}_r \equiv g_r(\sqrt{N/R_F^3}) = 0.2\varepsilon_F$). The non-resonant pairing interaction values we use are either $U = 0.001\omega_0$ ($\bar{U} \equiv U(N/R_F^3) = 0.35\varepsilon_F$) or $0.0015\omega_0$ ($\bar{U} = 0.52\varepsilon_F$). For the high-energy cutoff, we take $\omega_c = 161.5\hbar\omega_0$ ($\gg \varepsilon_F$).

The explicit calculations presented in this paper are for what is called a narrow Feshbach resonance, while all current ultracold Fermi gas experiments are done using broad Feshbach resonances. However, in a uniform Fermi gas, several quantities are found to have values very similar if viewed as a function of a_s , for both weak ($\bar{g}_r < \varepsilon_F$) and strong ($\bar{g}_r > \varepsilon_F$) Feshbach resonances. At the present time, numerical calculations are only able to deal with a narrow Feshbach resonance in the case of a trapped Fermi gas. This is due to the fact that one is limited to dealing with a finite number of excited states in a trap and this makes it difficult to deal with a broad Feshbach resonance, which couples molecules to Fermi atoms in very high-energy eigenstates. This approximate independence of the strength of the Feshbach resonance (for a given value of a_s) is thus very useful.

We first recall the standard case of two Fermi atoms interacting in a vacuum[48] with a bare interaction denoted by $-U$. In this case, the effective low-energy ($\omega = 0$) renormalized s -wave scattering length is given by

$$-\frac{4\pi a_s^{2b}}{m} = \frac{U}{1 - U \sum_{[0, \omega_c]} \frac{1}{2\varepsilon_{\mathbf{p}}}} \equiv U^R. \quad (4.1)$$

Effectively the renormalized interaction U^R incorporates all high energy scattering processes. In the absence of a Feshbach resonance ($g_r = 0$) and in a uniform gas, the gap equation (2.33) can be written in terms of this renormalized interaction as follows:

$$1 = U^R \sum_{[0, \omega_c]} \left[\frac{1}{2E_{\mathbf{p}}} \tanh \frac{E_{\mathbf{p}}}{2T} - \frac{1}{2\varepsilon_{\mathbf{p}}} \right]. \quad (4.2)$$

Here we have written the gap equation at finite temperatures. The summation in Eq. (4.2)

converges, so we can safely take $\omega_c \rightarrow \infty$. This gives a cutoff-independent gap equation as a function of the renormalized interaction U^R or, equivalently, the two-body scattering length a_s^{2b} defined in Eq. (4.1). As first discussed by Leggett[9] and Randeria[12], it is convenient to discuss the BCS-BEC crossover region in terms of the dimensionless parameter $(k_F a_s^{2b})^{-1}$. As the bare attractive interaction U increases, $(k_F a_s^{2b})^{-1}$ goes from $-\infty$ (BCS) to ∞ (BEC).

In the case of a Feshbach resonance, one can introduce a renormalized s -wave scattering length describing low energy atoms which is the analogue of Eq. (4.1), namely,

$$-\frac{4\pi a_s^{2b}}{m} \equiv \frac{U_{\text{eff}}^{2b}}{1 - U_{\text{eff}}^{2b} \sum_{[0, \omega_c]} \frac{1}{2\varepsilon_{\mathbf{p}}}}, \quad (4.3)$$

where the bare Feshbach resonance is described by

$$U_{\text{eff}}^{2b} \equiv U + \frac{g_r^2}{2\nu}. \quad (4.4)$$

Once can rewrite Eq. (4.3) in the form

$$-\frac{4\pi a_s^{2b}}{m} = U^R + \frac{(g_r^R)^2}{2\nu^R}, \quad (4.5)$$

which now involves the renormalized parameters for U , g_r , and 2ν (for details, see, for example, Sec. IV A of Ref. [2]). These low energy renormalized parameters can be directly measured.

However, in contrast to Eq. (4.2), the cutoff-independent energy gap equation in the presence of a Feshbach resonance is *not* given simply in terms of the usual two-body s -wave scattering length as defined in Eqs. (4.3) and (4.5). Instead, one finds[1, 2, 3, 4]

$$1 = U_{\text{eff}}^R \sum_{[0, \omega_c \rightarrow \infty]} \left[\frac{1}{2E_{\mathbf{p}}} \tanh \frac{E_{\mathbf{p}}}{2T} - \frac{1}{2\varepsilon_{\mathbf{p}}} \right], \quad (4.6)$$

where

$$\begin{aligned} U_{\text{eff}}^R &\equiv \frac{U_{\text{eff}}}{1 - U_{\text{eff}} \sum_{[0, \omega_c]} \frac{1}{2\varepsilon_{\mathbf{p}}}} \\ &\equiv U^R + \frac{(g_r^R)^2}{2\nu^R - 2\mu} \\ &\equiv -\frac{4\pi a_s}{m}. \end{aligned} \quad (4.7)$$

U_{eff} is defined in Eq. (2.10). We first restrict the following discussion to the case of a uniform Fermi superfluid. Comparing this new s -wave scattering length a_s involved in the

gap equation (4.6) with the two-body scattering length a_s^{2b} defined by Eqs. (4.3) and (4.5), we see that a_s depends crucially on the Fermi chemical potential μ . This in turn is a strong function of the threshold energy 2ν and hence will change value in the BCS-BEC crossover. One may think of a_s as including many-body effects related to the coupling of the fermions to molecular bosons[49]. We note in passing that it is wrong to simply use a_s^{2b} [given in Eq. (4.5)] in the gap equation (4.6) in the general case.

The fact that the cutoff-free gap equation (4.6) *only* depends on a_s , *irrespective of detailed values of the non-resonant interaction U and the Feshbach resonance strength g_r* , is very useful. In particular, a broad Feshbach resonance ($\bar{g}_r > \varepsilon_F$) and a narrow Feshbach resonance ($\bar{g}_r < \varepsilon_r$) give approximately the same values for T_c and $\tilde{\Delta}$ *for the same value of a_s* . As an example, we show in Fig. 1(a) the phase transition temperature T_c in the BCS-BEC crossover for a *uniform* gas for a broad and a narrow Feshbach resonances. In a broad Feshbach resonance, the BCS-BEC crossover occurs at the value of $\nu \gg \varepsilon_F$. In the case of a narrow Feshbach resonance, the crossover occurs at $\nu \sim \varepsilon_F$. However, when we express T_c as a function of $(k_F a_s)^{-1}$, both cases give almost the same result over the whole BCS-BEC crossover region, as shown in Fig. 1(a)[50]. In addition, Fig. 1(b) shows that the change from a gas of Fermi atoms to a molecular Bose gas in the BCS-BEC crossover is also almost the same for both large and small values of \bar{g}_r when viewed as a function of $(k_F a_s)^{-1}$. The region of $(k_F a_s)^{-1} > 0$ can thus be regarded as a BEC of molecular Bosons for both broad and narrow Feshbach resonances. Using a_s in Eq. (4.7), we find the same crossover physics irrespective of the width of the Feshbach resonance. This is useful since as we noted earlier, our numerical calculations are limited to $\bar{g}_r \lesssim \varepsilon_F$, while recent experiments deal with a broad Feshbach resonance. We also note that in the case of a broad Feshbach resonance, the crossover occurs at a value of $\nu \gg \varepsilon_F > \mu$. In this region, we can omit the chemical potential in Eq. (4.7) and then one finds $a_s \simeq a_s^{2b}$, the usual renormalized low-energy two-body scattering length which can be measured directly.

In contrast to T_c , the character of the Feshbach resonance (broad or narrow resonance) does show up somewhat when we consider the number of molecules N_M in Fig. 1(b). With increasing $(k_F a_s)^{-1}$ from the BCS side, Fig. 2(b) shows that the number of Feshbach molecules with a finite lifetime increases in the case of a *narrow* Feshbach resonance. Stable molecules ($N_B^{\gamma=0}$) become dominant in the region of negative chemical potential, $\mu < 0$ (see Fig. 2(a)). Although stable Cooper-pairs given by the $N_C^{\gamma=0}$ curve also exist in this region, we see that

$N_C^{\gamma=0} \ll N_B^{\gamma=0}$. Thus, in the case of a narrow Feshbach resonance (small \bar{g}_r), superfluidity in the region of $\mu < 0$ is largely associated with a BEC of stable Feshbach molecules.

On the other hand, in the case of a *broad* Feshbach resonance, the number of Cooper-pairs with a finite lifetime (N_C^{sc}) first rapidly increases as one increases $(k_F a_s)^{-1}$ [see Fig. 2(c)]. When $\mu < 0$, stable long lived Cooper-pairs ($N_C^{\gamma=0}$) become the dominant bound states. Below T_c , the tightly-bound molecules around $\mu \lesssim 0$ are now Cooper-pairs. As shown in Fig. 2(c), the Feshbach molecules ($N_B^{\gamma=0}$) eventually become dominant deep inside the BEC regime (defined by $(k_F a_s)^{-1} \sim 1$). The difference between the two cases is due the fact that, in a broad Feshbach resonance, the BCS-BEC crossover occurs around $\nu \gg \varepsilon_F$, where the formation/dissociation of Feshbach molecules only appears as a virtual process. In contrast, the crossover region is located in the region $\nu \lesssim \varepsilon_F$ in the case of a narrow Feshbach resonance, where a large number of Feshbach molecules can form as quasi-stable entities.

The preceding discussion was limited to a *uniform* Fermi superfluid. A discussion on T_c and the composite order parameter in terms of the scattering length a_s is also possible in a trapped gas, if we use the LDA[2, 51]. In this case, the spatially-dependent order parameter $\tilde{\Delta}(r)$ is self-consistently determined by the cutoff-dependent gap equation, given by

$$1 = U_{\text{eff}}(r) \sum_{[0, \omega_c]} \frac{1}{2E_{\mathbf{p}}(r)} \tanh \frac{E_{\mathbf{p}}(r)}{2T}. \quad (4.8)$$

Here $E_{\mathbf{p}}(r)$ is the energy of a BCS excitation with density and other quantities evaluated locally at position r . This is given by Eq. (2.32), with μ being replaced by $\mu(r) \equiv \mu - m\omega_0^2 r^2/2$. The bare pairing interaction strength at r in Eq. (4.8) is defined as

$$U_{\text{eff}}(r) \equiv U + \frac{g_r^2}{2\nu + (3/2)\omega_0 - 2\mu(r)}, \quad (4.9)$$

where we have included the zero point energy $(3/2)\omega_0$ for later discussions. From our preceding analysis, the LDA gap equation (4.8) can be written in a cutoff-independent form, but it now involves the renormalized pairing interaction given by

$$U_{\text{eff}}^R(r) \equiv \frac{U_{\text{eff}}(r)}{1 - U_{\text{eff}}(r) \sum_{[0, \omega_c]} \frac{1}{2\varepsilon_{\mathbf{p}}}}. \quad (4.10)$$

In particular, since $\mu(r=0) = \mu$, $U_{\text{eff}}^R(r=0)$ equals U_{eff}^R given in Eq (4.7) [apart from the zero point energy term $(3/2)\omega_0$ in Eq. (4.9)]. Thus, recalling that T_c in the LDA[2] is

determined by the gap equation (4.8) at $r = 0$, we conclude that the crossover behavior of T_c and $\tilde{\Delta}(r = 0)$ at the center of the trap can be described (as in a uniform Fermi gas) as functions of the renormalized scattering length a_s defined in Eq. (4.7). Indeed, Fig. 3(a) shows that both narrow and broad Feshbach resonance cases give almost the same T_c as a function of $(k_F a_s)^{-1}$ in the whole BCS-BEC crossover regime.

As in a uniform gas discussed above, in a trap some quantities will depend on the strength of the Feshbach resonance. The LDA gap equation (4.8) involves a position-dependent $a_s(r)$ because of the spatial dependence of $\mu(r)$. In a broad Feshbach resonance ($\bar{g}_r \gg \varepsilon_F$), the crossover occurs at $\nu \gg \varepsilon_F$, so that $\mu(r)$ ($\sim \varepsilon_F$) can be neglected in this regime. On the other hand, $U_{\text{eff}}(r)$ decreases as we go from the center of the trap in the case of a narrow Feshbach resonance ($\bar{g}_r < \varepsilon_F$), since now the crossover occurs at $\nu \sim \varepsilon_F$ and hence $\mu(r)$ cannot be ignored in $U_{\text{eff}}(r)$. This explains why the total number of molecules is slightly smaller in the case of a narrow Feshbach resonance, as shown in Fig. 3(b)

In this paper, we present results as a functions of the renormalized uniform gas scattering length a_s in Eq. (4.7), with the result that the theory is approximately cutoff-free within LDA. The dependence on $(k_F a_s)^{-1}$ also gives a description for Fermi superfluids around the center of the trap, irrespective of the width of the Feshbach resonance. We refer to the region of $(k_F a_s)^{-1} < 0$ as the BCS regime and the region of $(k_F a_s)^{-1} > 0$ as the BEC regime. We note that the “real” or bare pairing interaction in the gap equation is *not* $4\pi a_s/m$, but $-U_{\text{eff}}$ defined in Eq. (2.10). This is always *attractive* even in the positive (BEC) region of $a_s > 0$, as we show in Fig. 4(a). In Fig. 4(b), we give the relation between a_s and ν , for the parameters g_r and U used in this paper. In the numerical results discussed in this paper, for the convenience of the reader, we give both the value of ν as well as the corresponding value of $(k_F a_s)^{-1}$.

V. EQUILIBRIUM PROPERTIES IN THE CROSSOVER REGION

Figure 5 shows the calculated atomic density profile at different places in the BCS-BEC crossover region at $T = 0$. In the BCS regime shown in Fig. 5(a), the number of Fermi atoms is much larger than the number of (Feshbach) molecules. Although these atoms form Cooper-pair bosons, the Pauli exclusion principle is still relevant. As a result, the Fermi gas spreads out to a distance of the order of the Thomas-Fermi radius R_F , just as in the case of

a trapped non-interacting Fermi gas. We recall that in contrast to bosons, interactions have a negligible effect on the density profile of a trapped Fermi gas in the normal phase. The relative number of Cooper-paired fermions $[n_F(r)]$ and bound (Feshbach) dimers $[n_M(r)]$ continuously changes as the threshold energy 2ν is lowered (or $(k_F a_s)^{-1}$ increases). On the BCS side of the crossover regime shown in Fig. 5(b), the molecular density $n_M(r)$ has become very large in the center of the trap. This shows that the Pauli exclusion principle, as expected, is less important in this region where Bose molecules start to dominate. However, the Fermi atoms still dominate for $r \gtrsim 0.2R_F$. This feature persists on the BEC side of crossover regime shown in Fig. 5(c), where $n_F(r)$ is seen to be dominant for $r \gtrsim 0.3R_F$. The tail of the density profile consisting of unpaired atoms finally disappears in Fig. 5(d), where almost all the atoms have formed Feshbach molecules.

Figure 6 shows how the Fermi chemical potential μ changes in the BCS-BEC crossover. As one approaches the BEC regime, μ decreases from the weak-coupling (BCS) result given by $\mu \simeq \varepsilon_F$ ($= 31.5\omega_0$ in our case). In the BEC regime, the molecular Bose chemical potential $\mu_M = 2\mu$ approaches the lowest molecular energy, given by $2\nu + (3/2)\omega_0$, as shown in the inset in Fig. 6. We note that this limiting case of $\mu_M = 2\nu + (3/2)\omega_0$ is just the condition for the BEC of a non-interacting Bose gas in a harmonic trap.

In Fig. 6, the Fermi chemical potential is seen to go through zero at $(k_F a_s)^{-1} \simeq 0.65$, which corresponds to $\nu = 0$. To understand this, let us consider the case of a *uniform* gas. In this case, the single-particle excitation spectrum is given by the usual BCS expression (but now with the composite order parameter $\tilde{\Delta}$) [3, 9, 12, 30],

$$E_{\mathbf{p}} = \sqrt{(\varepsilon_{\mathbf{p}} - \mu)^2 + \tilde{\Delta}^2}. \quad (5.1)$$

In the weak-coupling BCS regime, where μ is positive, the energy gap of the BCS excitations at the Fermi energy is equal to $|\tilde{\Delta}|$. However, this relation is no longer valid when μ is negative, as in the strong-coupling crossover regime[9, 13]. In this regime, the energy gap is given by

$$E_g = \sqrt{\mu^2 + \tilde{\Delta}^2}. \quad (5.2)$$

In the BEC limit ($\nu \rightarrow -\infty$), the composite order parameter is described by a pure BEC condensate of molecules, given by $\tilde{\Delta} \rightarrow g_r \sqrt{N/2}$. In the same limit, the chemical potential approaches the threshold energy $\mu \simeq \nu \rightarrow -\infty$. Thus, the excitation gap E_g given by Eq.

(5.2) approaches $|\nu|$. This makes sense, since 2ν (< 0) is the lowest molecular energy, and hence $2|\nu|$ is the excitation energy to dissociate a molecule into *two* Fermi atoms.

In a trapped gas, within the LDA, the chemical potential μ and the order parameter $\tilde{\Delta}$ in Eq. (5.2) are replaced by the position-dependent ones, $\mu(r) \equiv \mu - m\omega_0^2 r^2/2$ and $\tilde{\Delta}(r)$, respectively. In the extreme BEC limit ($\nu \rightarrow -\infty$), the lowest single-particle excitation energy is given as the energy to dissociate a molecule into two Fermi atoms and put them at the lowest (unpaired) fermion state. In the LDA, this lowest state is at $r = 0$, because the trap potential has its minimum at the center [$V_{\text{trap}}^{\text{F}}(r = 0) = 0$]. This again leads to $E_g \sim |\mu| \sim |\nu|$ in the BEC limit (when $\tilde{\Delta}(0) \ll |\mu|$). As a result, we find that $(k_{\text{F}} a_s)^{-1} \simeq 0.65$ (at which $\mu = 0$) gives a characteristic scattering length which separates the region dominated by weakly-bound Cooper-pairs ($\mu > 0$) and the region dominated by tightly-bound molecules ($\mu < 0$). Equivalently, this boundary occurs at $\nu = 0$.

Figure 7 shows the profile of composite order parameter $\tilde{\Delta}(r)$. As expected from Fig. 5, $\tilde{\Delta}(r)$ is dominated by the Cooper-pair component $\Delta(r)$ in the BCS regime shown in panel 7(a). This calculated profile agrees with previous results in the BCS limit, as obtained by Bruun and co-workers[37]. However, in the presence of a Feshbach resonance, even in the BCS regime, the molecular condensate $\phi_M(r)$ is found to be finite everywhere $\Delta(r)$ is finite, due to the identity given in Eq. (2.6). In an ideal Bose gas BEC, $\phi_M(r)$ is simply proportional to the ground state wavefunction of the harmonic potential given by Eq. (2.23). However, since the molecular bosons are strongly hybridized with the Fermi atoms by the Feshbach resonance, in the BCS regime, we find that $\phi_M(r)$ is no longer given by the ground state of the harmonic potential as in Eq. (2.23). Indeed, as shown in Fig. 8(a), $\phi_M(r)$ in this regime is given by a superposition of excited molecular states ($n \geq 1$), as indicated in Eq. (2.21). The molecular condensate $\phi_M(r)$ continuously increases in magnitude as one approaches the BEC regime, as shown in Figs. 7(b) and (c). At the same time, Fig. 8 shows that the contribution of excited states ($n \geq 1$) decreases, indicating that $\phi_M(r)$ approaches the ideal BEC described by Eq. (2.23). However, because of the identity in Eq. (2.6), the Cooper-pair component $\Delta(r)$ remains finite even in the BEC regime. Indeed, as shown in Fig. 7(d), $\Delta(r = 0) \simeq 15\omega_0$ when $\nu = 0$.

In Fig. 9, we compare the total atomic density profile $n(r) = 2n_{\text{M}}(r) + n_{\text{F}}(r)$ with the profile of the composite order parameter $\tilde{\Delta}(r)$, which clearly shows that the composite order parameter is always finite in the region where $n(r)$ is finite. In addition, we expect that

$n(r) \simeq |\phi_M(r)|^2$ in the BEC regime. This is confirmed by the calculated values shown in the inset in Fig. 9(b), which show that $n(r) \simeq |\tilde{\Delta}(r)|^2$.

We note that when the LDA is used in calculating the density profile as well as the order parameter at $T = 0$, it has been shown that the LDA is a good approximation in the BCS regime[37]. In contrast, the shrinkage of the density profile $n(r)$ shown in Fig. 7, as well as the profile of the composite order parameter $\tilde{\Delta}(r)$, is poorly overestimated by the LDA[51] as we enter the BEC regime. This is because the LDA underestimates the kinetic energy, which results in the density profile of atoms spreading out more.

At $T = 0$, such an LDA calculation correctly predicts that the resulting composite order parameter is finite in all regions where $n(r)$ is finite. This reflects the fact that the Fermi surface is unstable against an infinitesimally weak attractive interaction at $T = 0$, which leads to a superfluid phase transition everywhere (as long as $n(r)$ is positive) in a trap in the LDA. However, this situation is no longer satisfied at finite temperatures. As we have discussed in Ref. [2], only the center of the trap ($r = 0$) is in the superfluid phase *just below* T_c in the LDA, with this superfluid region becoming wider with decreasing temperatures. Thus, for $0 < T < T_c$, an LDA calculation predicts a spatial region where the order parameter vanishes, even though the particle density is still finite. (This feature is shown in Fig. 1 of Ref. [29].) However, the presence of such a “two-phase” trapped Fermi gas (superfluid at the center and normal phase at the edge of the trap) is clearly an artifact of the LDA. In fact, the entire gas is in the superfluid phase below T_c , with $\tilde{\Delta}(r)$ finite everywhere where $n(r)$ is finite.

VI. SINGLE-PARTICLE EXCITATIONS IN THE CROSSOVER REGION

Figure 10 shows single-particle density-of-states $N(\omega)$ given in Eq. (3.8). One sees that the excitation spectrum in a Fermi superfluid has a finite energy gap ($\equiv E_g$). Although the pairing interaction becomes stronger with decreasing threshold energy 2ν , the magnitude of $E_g \sim 1.2\omega_0$ is almost the same in panels (a) and (b) of Fig. 10. We also note that there is characteristic sharp increase or shoulder around E_g . Recalling the case of a *uniform* BCS superfluid (where the energy gap is equal to $|\tilde{\Delta}|$), one has the well-known result

$$N(\omega) = \rho(\varepsilon_F) \frac{\omega}{\sqrt{\omega^2 - \tilde{\Delta}^2}} \Theta(\omega - |\tilde{\Delta}|), \quad (6.1)$$

where $\Theta(x)$ is the step function. The normal-state density of states is given by $\rho(\omega) \equiv \frac{m\sqrt{2m\omega}}{2\pi^2}$. [We have approximated this by the value at the Fermi energy, $\omega = \varepsilon_F$, in Eq. (6.1). This is a good approximation in the BCS limit. The more correct expression for $N(\omega)$, including the effect of the energy-dependence of $\rho(\omega)$, is given in Ref. [3].] Equation (6.1) predicts that $N(\omega)$ is singular at $\omega = |\tilde{\Delta}|$. The sudden increase in $N(\omega)$ at $\omega = E_g$ in the *trapped* gas shown in Figs. 10(a) and (b) may be viewed as the remnant of this singular behavior of the single-particle excitations in the uniform BCS case.

Figure 10(c) shows the change in the density of states $N(\omega)$ as we enter into the BEC region ($\nu < 0$). One finds that the energy gap now sharply increases ($E_g \simeq 5\omega_0$) and the sudden jump in the magnitude of $N(\omega)$ at the energy gap E_g is absent.

In Fig. 11, we plot the single-particle excitation gap E_g in the BCS-BEC crossover region[53]. This figure shows that E_g rapidly increases when the chemical potential μ becomes negative [$(k_F a_s)^{-1} > 0.65$]. In this region, $2E_g$ is the dissociation energy of a molecule. This energy $2E_g \simeq |\mu_M| \simeq 2|\nu|$ becomes large as we decrease the threshold energy $2\nu \rightarrow -\infty$. Indeed, we find that E_g approaches $|\mu|$ (given by the dashed line in Fig. 11) when we take $\mu \rightarrow -\infty$, which is consistent with Eq. (5.2) valid for a uniform gas. We also see from Fig. 12 that the number of molecules becomes much larger than the number of Fermi atoms for $\nu < 0$ or $(k_F a_s)^{-1} > 0.65$, as expected.

One can understand (in the case of a uniform gas) why the “coherence peak” (i.e., the sudden jump) in $N(\omega)$ at E_g is absent in the crossover region shown in Fig. 10(c). In the BEC region one finds (see Eq. (5.4) of Ref. [3])

$$N(\omega) = \frac{m\sqrt{2m}}{4\pi^2} \left(1 + \frac{\omega}{\sqrt{\omega^2 - \tilde{\Delta}^2}}\right) (\sqrt{\omega^2 - \tilde{\Delta}^2} + \mu)^{1/2} \Theta(\omega - \sqrt{\mu^2 + \tilde{\Delta}^2}), \quad (6.2)$$

where the factor $(\sqrt{\omega^2 - \tilde{\Delta}^2} + \mu)^{1/2}$ comes from the normal state density-of-states $\rho(\omega) \propto \sqrt{\omega}$. When μ is negative, the threshold energy of the $N(\omega)$ is determined not by the factor $\sqrt{\omega^2 - \tilde{\Delta}^2}$, but by the threshold energy of the normal DOS $\rho(\omega)$. This leads to the step function in Eq. (6.2). As a result, the density-of-states $N(\omega)$ of a Fermi superfluid is finite only for $\omega \geq \sqrt{\mu^2 + \tilde{\Delta}^2}$. The expected coherence peak at $\omega = |\tilde{\Delta}| < \sqrt{\mu^2 + \tilde{\Delta}^2}$ actually occurs in a region where $N(\omega)$ vanishes.

When we compare the single-particle excitation gap E_g for $\mu > 0$ in Fig. 11 with the magnitude $\tilde{\Delta}(r=0)$ of the composite order parameter shown in Fig. 13, we see that $E_g \ll |\tilde{\Delta}(0)| \sim \varepsilon_F$ in the crossover region. Since the excitation gap E_g equals the order parameter

(when $\mu > 0$) in a uniform gas, this difference clearly originates from the inhomogeneity of a superfluid Fermi gas in a trap. To understand the origin of this very small value of the single-particle excitation gap E_g in a *trapped* superfluid Fermi gas, it is very useful to compare $N(\omega)$ and the local density of states $N(\omega, \mathbf{r})$ given by the expression in Eq. (3.9). Figure 14(b) shows that no low energy spectral weight comes from the center of the trap. In fact, panel (d) clearly shows that the low-energy spectral weight in $N(\omega)$ shown in panel (a) mainly comes from the region $r \sim 0.6R_F$, which is close to the bottom of the *effective potential well* composed of the (composite) pair potential $\tilde{\Delta}(r)$ and the harmonic trap measured from the chemical potential μ , given by $V_{\text{trap}}^{\text{eff}}(r) \equiv (V_{\text{trap}}^F(r) - \mu)\Theta(V_{\text{trap}}^F(r) - \mu)$ [see the inset of Fig. 14(b)]. Strictly speaking, this effective potential is a combination of an ordinary (diagonal) and an anomalous (off-diagonal) potential in the BdG equations. This situation is analogous to the boundary problem in superconductivity, as schematically indicated in Fig. 15. As first discussed by de Gennes and Saint-James[52] in the context of superconductivity, “Andreev” bound states can appear well below the bulk energy gap ($\sim \tilde{\Delta}$), around the minimum of the effective potential well. Thus E_g may be viewed as the energy of the lowest Andreev bound state formed in the effective potential well [= $\tilde{\Delta}(r) + V_{\text{trap}}^{\text{eff}}(r)$]. These are also called the “in-gap” states[57].

The role of such surface excitations was first discussed by Baranov[57] in connection with a BCS superfluid gas in a trap, using the WKB semi-classical solution of the BdG equations. More recent papers in the context of the BCS-BEC crossover are by Kinnunen, Rodriguez, and Törmä[29] using LDA, and by Heiselberg[58] using the WKB approximation. We note that bound state energies decrease when the effective potential width d in Fig. 15(b) increases. In a trapped Fermi gas, the analogous effective potential well becomes wider as we enter the crossover regime because the spatial width of the composite order parameter $\tilde{\Delta}(r)$ shrinks in this region, as shown in Fig. 7. In addition, the decrease of chemical potential μ leads to a more gradual slope of the diagonal potential $V_{\text{trap}}^{\text{eff}}(r)$ around $V_{\text{trap}}^{\text{eff}}(r) = 0$. These are the reasons why E_g slightly decreases (see the inset of Fig. 11) with increasing $(k_F a_s)^{-1}$, in the region $0.65 > (k_F a_s)^{-1} > 0$. We note that the lowest Andreev bound state energy level does not determine E_g once we are in the BEC region ($\mu < 0$). In this case, $2E_g$ is dominated by the dissociation energy of tightly bound molecules and thus we find $E_g \sim |\mu| \sim |\nu|$ ($\nu \rightarrow -\infty$) in Fig. 11.

In connection with the WKB approximation[57, 58], we remark that this should be quite

good in the extreme BCS limit, where there is still a well-defined Fermi surface. However, this approach seems less justified in the crossover region, where the important single-particle states are no longer close to the Fermi energy. Further studies are needed of the validity of the semi-classical approximation to the BdG equations in the crossover region.

VII. RF-TUNNELING SPECTROSCOPY IN A TRAPPED FERMION SUPERFLUID

In this section, we discuss recent work using rf-tunneling spectroscopy. As with any tunneling experiment, this clearly gives information about the single-particle excitations in fermion superfluids[27, 29, 54, 55, 56, 58, 59, 60]. In particular, one can extract information about both the energy gap of the single particle excitations as well as the value of the pair order parameter, but this can only be done by comparison with theoretical calculations. The rf-tunneling spectroscopy cross-section is calculated by considering the tunneling current induced by laser radiation. In the rotational wave approximation, the tunneling Hamiltonian is given by[29, 54, 55, 56]

$$\begin{aligned}
H_t &= H_t^F + H_t^M \\
&= t_F \int d\mathbf{r} \left[e^{i(\mathbf{q}_L \cdot \mathbf{r} - \omega_L t)} \Psi_a^\dagger(\mathbf{r}) \Psi_\uparrow(\mathbf{r}) + h.c. \right] \\
&+ t_M \int d\mathbf{r} \left[e^{i(\mathbf{q}_L \cdot \mathbf{r} - \omega_L t)} \Psi_a^\dagger(\mathbf{r}) \Psi_\downarrow^\dagger(\mathbf{r}) \Phi(\mathbf{r}) + h.c. \right].
\end{aligned} \tag{7.1}$$

Here \mathbf{q}_L and ω_L represent the momentum and frequency of the laser light, respectively. The first term H_t^F describes the usual tunneling of an atom in the \downarrow -spin state to another hyperfine state described by the fermion field operator $\Psi_a(\mathbf{r})$, with a strength given by the tunneling matrix element t_F . (We assume that t_F has no spatial dependence.) This new hyperfine state Ψ_a is described by the Hamiltonian

$$H_a = \int d\mathbf{r} \Psi_a^\dagger(\mathbf{r}) \left[-\frac{\nabla^2}{2m} + \omega_a - \mu_a + V_{\text{trap}}^F \right] \Psi_a(\mathbf{r}), \tag{7.2}$$

where ω_a is the threshold energy and μ_a is the chemical potential of this state. In Eq. (7.2), we assume that atoms in this state are non-interacting and feel the same trap frequency as the other hyperfine states \uparrow, \downarrow . The second term H_t^M in Eq. (7.1) describes the tunneling into state Ψ_a associated with the dissociation of a bosonic molecule, with the matrix element t_M . This process is the signature of a Feshbach resonance. In the superfluid phase at $T = 0$,

the Bose quantum field operator $\Phi(\mathbf{r})$ can be replaced by the macroscopic wavefunction $\phi_M(\mathbf{r})$. In this case, the molecule component in Eq. (7.1) reduces to

$$H_t^M = t_M \int d\mathbf{r} \left[e^{i(\mathbf{q}_L \cdot \mathbf{r} - \omega_L t)} \phi_M(\mathbf{r}) \Psi_a^\dagger(\mathbf{r}) \Psi_\downarrow^\dagger(\mathbf{r}) + h.c. \right]. \quad (7.3)$$

The tunneling current operator is obtained from $\hat{I}(t) = \dot{N}_a(t) = i[H, N_a(t)]$, where $N_a \equiv \int d\mathbf{r} \Psi_a^\dagger(\mathbf{r}) \Psi_a(\mathbf{r})$ is the number operator of the Ψ_a -state (for details, see, for example, Chap. 9 of Ref. [46]). The resulting current operators originating from H_t^F and H_t^M are given by, respectively,

$$\hat{I}_F(t) \equiv -it_F \int d\mathbf{r} \left[e^{i(\mathbf{q}_L \cdot \mathbf{r} - \omega_L t)} \Psi_a^\dagger(\mathbf{r}) \Psi_\uparrow(\mathbf{r}) - h.c. \right], \quad (7.4)$$

$$\hat{I}_M(t) \equiv -it_M \int d\mathbf{r} \left[e^{i(\mathbf{q}_L \cdot \mathbf{r} - \omega_L t)} \phi_M(\mathbf{r}) \Psi_a^\dagger(\mathbf{r}) \Psi_\downarrow^\dagger(\mathbf{r}) - h.c. \right]. \quad (7.5)$$

Assuming the tunneling matrix elements t_F and t_M are small, we can evaluate the tunneling current using first order perturbation in H_t . The current associated with the usual tunneling term H_t^F induced by the rf-field is given by (we set $\mathbf{q}_L = 0$)

$$I_F(\omega) = \langle \hat{I}_F(\omega) \rangle = 2t_F^2 \text{Im} \int d\mathbf{r} d\mathbf{r}' \Pi_F(\mathbf{r}, \mathbf{r}', -\omega), \quad (7.6)$$

where

$$\omega \equiv \omega_L - \omega_a - \mu + \mu_a \quad (7.7)$$

defines the effective *detuning frequency*. The two-particle Green's function $\Pi_F(\mathbf{r}, \mathbf{r}', \omega)$ in Eq. (7.6) is obtained from the analytic continuation[46] of the thermal Green's function

$$\begin{aligned} \Pi_F(\mathbf{r}, \mathbf{r}', i\nu_n) &\equiv - \int_0^\beta d\tau e^{i\nu_n \tau} \langle T_\tau \{ \Psi_a^\dagger(\mathbf{r}, \tau) \Psi_\uparrow(\mathbf{r}, \tau) \Psi_\uparrow^\dagger(\mathbf{r}', \tau) \Psi_a(\mathbf{r}', \tau) \} \rangle \\ &= \frac{1}{\beta} \sum_{i\omega_m} G_{11}(\mathbf{r}, \mathbf{r}', i\omega_m + i\nu_n) G_a(\mathbf{r}', \mathbf{r}, i\omega_m). \end{aligned} \quad (7.8)$$

Here, G_a is the single-particle thermal Green's function for the Ψ_a state quantum field operator,

$$G_a(\mathbf{r}, \mathbf{r}', i\omega_m) = \sum_{nlm} \frac{Y_{lm}(\hat{\theta}) R_{nl}^F(r) R_{nl}^F(r') Y_{lm}^*(\hat{\theta}')}{i\omega_m - \xi_{nl}^F}. \quad (7.9)$$

Here $\xi_{nl}^F = \omega_0(2n + l + 3/2) - \mu_a$ describe the energy levels of the Ψ_a atomic hyperfine states. We note that Eq. (7.9) does not explicitly involve the threshold energy ω_a or the chemical potential μ_a , because these have been included in the effective detuning ω as defined in Eq. (7.7). Hopefully, there will be no confusion with the label of the Fermi Matsubara frequency $\omega_m = \pi T(2m + 1)$ and the azimuthal quantum number m .

We substitute the diagonal Green's functions G_{11} in Eq. (3.4) and G_a in Eq. (7.9) into Eq. (7.8), and carry out the Matsubara ω_m -frequency summation in the usual way[46]. After doing the analytic continuation to real frequencies, we obtain (at $T = 0$ and $\omega > 0$)

$$I_F(\omega) = 2\pi t_F^2 \sum_l (2l+1) \sum_{j=0}^{N_l} \sum_{n=0}^{N_l} |W_{n+1, \bar{N}_l+j}^l|^2 \Theta(\xi_{nl}^F) \delta(\xi_{nl}^F + E_{jl}^F - \omega), \quad (7.10)$$

where E_{jl}^F is the energy eigenvalue given by the self-consistent solutions of the BdG equations.

The tunneling current from molecules $I_M(\omega) = \langle \hat{I}_M(\omega) \rangle$ can be calculated in the same way. Within first order perturbation in H_f^M , we find

$$I_M(\omega) = 2t_M^2 \text{Im} \int d\mathbf{r} d\mathbf{r}' \phi_m(\mathbf{r}) \phi_m(\mathbf{r}') \Pi_B(\mathbf{r}, \mathbf{r}', -\omega), \quad (7.11)$$

where

$$\begin{aligned} \Pi_B(\mathbf{r}, \mathbf{r}', i\nu_n) &\equiv - \int_0^\beta d\tau e^{i\nu_n \tau} \langle T_\tau \{ \Psi_a^\dagger(\mathbf{r}, \tau) \Psi_\downarrow^\dagger(\mathbf{r}, \tau) \Psi_\downarrow(\mathbf{r}') \Psi_a(\mathbf{r}') \} \rangle \\ &= \frac{1}{\beta} \sum_{i\omega_m} G_{22}(\mathbf{r}, \mathbf{r}', i\omega_m + i\nu_n) G_a(\mathbf{r}', \mathbf{r}, i\omega_m). \end{aligned} \quad (7.12)$$

Carrying out the ω_m -frequency summation in Eq. (7.12) and the analytic continuation, we obtain

$$I_M(\omega) = 2\pi t_M^2 \sum_l (2l+1) \sum_{j=0}^{N_l} \sum_{n=0}^{N_l} |\Xi_{nj}^F|^2 \Theta(\xi_{nl}^F) \delta(\xi_{nl}^F + E_{jl}^F - \omega), \quad (7.13)$$

where the matrix element is given by

$$\Xi_{nl}^F \equiv \sum_{n'=0}^{N_l} W_{\bar{N}_l+n', \bar{N}_l+j}^l \int_0^\infty r^2 dr R_{nl}^F(r) \phi_M(r) R_{n'l}^F(r). \quad (7.14)$$

The analogue of these results were first worked out by Törmä and co-workers[29, 54, 55, 56], both for a uniform gas and a trapped gas within the LDA. Refs. [29, 56] only include the molecular tunneling current originating from the dissociation of *excited* molecules, which only becomes important at finite temperatures close to T_c . In the case of $T = 0$, which we are considering, all the molecules are Bose-condensed. In this case, the contribution in Eq (7.13) associated with the dissociation of the *Bose-condensed* molecules gives the dominant contribution to the molecular current.

In order to illustrate the physics of the preceding expressions for $I_F(\omega)$ and $I_M(\omega)$, it is useful to consider a *uniform* superfluid Fermi gas at $T = 0$. In this case, it is convenient to evaluate $I_F(\omega)$ and $I_M(\omega)$ in momentum space. In a uniform gas, the two-particle Green's

function Π in Eq. (7.6) only depends on the relative coordinate as $\Pi(\mathbf{r} - \mathbf{r}', -\omega)$, so that Eq. (7.6) can be written as

$$I_F(\omega) = 2t_F^2 \frac{1}{\beta} \sum_{\mathbf{p}, i\omega_m} \text{Im} \left[G_{11}(\mathbf{p}, i\omega_m + i\nu_n) G_a(\mathbf{p}, i\omega_m) \right], \quad (7.15)$$

where G_{11} is given in Eq. (2.31), and $G_a^{-1}(\mathbf{p}, i\omega_m) \equiv i\omega_m - \xi_{\mathbf{p}}$ is the single-particle Green's function of a free uniform Fermi gas of atoms in the hyperfine state 'a'. After doing the ω_m - and \mathbf{p} -summations, one finds[54]

$$I_F(\omega) = \pi t_F^2 \rho \left(\Omega = \frac{1}{2} \frac{\omega^2 - \tilde{\Delta}^2}{\omega} + \mu \right) \frac{\tilde{\Delta}^2}{\omega^2} \Theta(\omega - \tilde{\Delta}) \Theta \left(\frac{1}{2} \frac{\omega^2 - \tilde{\Delta}^2}{\omega} + \mu \right). \quad (7.16)$$

Here, $\rho(\Omega) \propto \sqrt{\Omega}$ is normal state density-of-states given below Eq. (6.1). Equation (7.16) clearly has a peak at the energy gap given by $\omega = |\tilde{\Delta}|$ as long as $\mu > 0$ (BCS region). On the other hand, when $\mu < 0$ (BEC region), the threshold energy is given by the last factor in Eq. (7.16),

$$\omega_{\text{th}} = |\mu| + \sqrt{\mu^2 + \tilde{\Delta}^2}, \quad (7.17)$$

rather than $\omega_{\text{th}} = |\tilde{\Delta}|$. In this BEC limit, the expression in Eq. (7.17) approaches the binding energy of a molecular boson as $\omega_{\text{th}} \rightarrow 2|\mu| \simeq 2|\nu|$, which is twice as large as the threshold energy (or energy gap) of the single-particle Fermi excitations (in a uniform gas). As one might expect, the threshold energy of the rf-induced tunneling current $I_F(\omega)$ continuously changes from the single-particle excitation gap $|\tilde{\Delta}|$ in the BCS regime to the threshold of the two-particle continuum in the BEC limit. In a trap, the tunneling current $I_F(\omega)$ in LDA[29] is given simply by the spatial integration over Eq. (7.16), where $\tilde{\Delta}(\mathbf{r})$ and $\mu(\mathbf{r}) \equiv \mu - \frac{1}{2}m\omega_0^2 r^2$ now depend on the position \mathbf{r} . The sharp peak at the excitation threshold then becomes broadened, as first discussed in Ref.[29].

Figure 16 shows our calculated results for the rf-induced current $I_F(\omega)$ in the BCS-BEC crossover at $T = 0$ in a *trapped* gas. Since we take into account the discrete energy levels of the harmonic trap potential (see Fig. 10), the spectrum shows rapid oscillations. In panel (a) describing the BCS region, one sees that the lowest tunneling current frequency is at $\omega \simeq 0.08\varepsilon_F$ [61]. This corresponds to the single-particle excitation gap E_g discussed in Section VI. A broad peak is also evident, centered at $\omega \sim 0.3\varepsilon_F$. This peak energy is seen to decrease as one enters the crossover region [panel (b) of Fig. 16]. Since the profile of the composite order parameter shrinks and the chemical potential μ decreases in this regime

(see Figs. 6 and 7), the width of the combined potential well [$\tilde{\Delta}(r) + V_{\text{eff}}^{\text{trap}}(r)$, see also the inset in Fig. 14(b)] increases. In this case, a large number of low-energy excitations appear, which are localized at the minimum of the potential well. These low energy excitations lead to the large value of $I_F(\omega)$ at low ω , as shown in Fig. 16(b). In contrast, once we enter the BEC regime, the single-particle excitation gap E_g quickly becomes large (see Fig. 11). This shows up in the rf-tunneling currents in panels (c) and (d), where the low-energy Andreev surface excitations no longer determine the pair threshold in $I_F(\omega)$, even though these states still exist. In Fig. 16(d), we see the threshold energy of the Fermi spectrum becomes quite large, at $\omega_{\text{th}} \simeq 2\varepsilon_F$, a result of being in the BEC region. This value is approximately twice as large as E_g (see Fig. 11) for this value of ν , and is consistent with the discussion given above for the case of a uniform superfluid.

For comparison, Fig. 17 shows the rf-tunneling spectroscopy calculated using the LDA, which is given by [see Eq. (7.16)]

$$I_F(\omega) = \pi t_F^2 \int d\mathbf{r} \rho \left(\Omega = \frac{1}{2} \frac{\omega^2 - \tilde{\Delta}(r)^2}{\omega} + \mu(r) \right) \frac{\tilde{\Delta}(r)^2}{\omega^2} \Theta(\omega - \tilde{\Delta}(r)) \Theta \left(\frac{1}{2} \frac{\omega^2 - \tilde{\Delta}(r)^2}{\omega} + \mu(r) \right). \quad (7.18)$$

Here $\mu(r) = \mu - \frac{1}{2} m \omega_0^2 r^2 + \frac{U}{2} n_F(r)$, where $\frac{U}{2} n_F(r)$ is the Hartree term. The values of μ , $\tilde{\Delta}(r)$, and $n_F(r)$ which are used in Eq. (7.18) are obtained by solving the BdG coupled equations in a self-consistent manner, as discussed in earlier sections.

Comparing Fig. 17 with Fig. 16, we find that when these self-consistent solutions of the BdG equations are used, the LDA gives a good overall approximation in the whole crossover regime for the rf-tunneling spectroscopy. However, it does not give the *true* energy gap ($E_g \sim 0.08\varepsilon_F \ll \varepsilon_F$) in the BCS regime, in contrast to the microscopic results shown in Figs. 16(a) and (b). Since this energy gap E_g originates from the Andreev bound states, it is no surprise that an LDA calculation does not reproduce it.

Although the peak energy in the tunneling current is very small in Fig. 16(b), this does *not* mean that the “average” magnitude of the composite order parameter is small. When we extract the contribution coming from the central region of the trap ($0 \leq r \leq r_c$, where $r_c \ll R_F$), $I_F(\omega)$ has a peak at a high energy, reflecting the large magnitude of $\tilde{\Delta}(r \sim 0)$. This is shown in Fig. 17(b) for the case $r_c = 0.3R_F$ (line 1), where $I_F^{\text{LDA}}(\omega)$ has a peak around $\omega \sim \varepsilon_F$. In this restricted spatial region ($0 \leq r \leq 0.3R_F$), $\tilde{\Delta}(r)$ is of the order of the Fermi energy, as shown in the inset of Fig. 17(b). As one increases r_c , the contribution of

the low-energy excitations localized around the surface region of the cloud begins to “hide” this high energy peak. When we take $r_c = 0.6R_F$ in Fig. 17(b) (the line 2), the peak in the spectrum is still dominated by the low energy excitations. It would be very useful in future experiments if one could measure the rf-tunneling current from the central region of the trap. In principle, such selective measurements could give detailed information about the spatial dependence of $\tilde{\Delta}(r)$.

When the profile of the composite order parameter spreads out up to R_F (namely, when $\tilde{\Delta}(r)$ is large even close to the trap edge), one expects that the effect of high energy excitations with an energy gap close to $\tilde{\Delta}(r=0)$ will dominate over low-energy excitations in the rf-spectrum $I_F(\omega)$. To confirm this expectation, we show a calculation in Fig. 18 using an ad-hoc model for $\tilde{\Delta}(r)$ shown in the inset. One finds that, as expected, the rf-tunneling spectrum for this broad order parameter has a high-energy peak at $\omega \sim \tilde{\Delta}(0) \sim \varepsilon_F$. This kind of slowly decreasing $\tilde{\Delta}(r)$ might be obtained when the effective repulsive molecule-molecule is strong, which our calculations have ignored. We also note that our explicit calculations are for a *narrow* Feshbach resonance, in which case molecules are dominant in the crossover region. [Our self-consistent expression for $\tilde{\Delta}(r)$ is shown in the inset of Fig. 17(b).] In a *broad* Feshbach resonance, where Cooper-pairs are dominant in the crossover regime and the size of these Cooper-pairs is still fairly large, such a broad profile of $\tilde{\Delta}(r)$ may be possible. In the recent calculations of the rf-tunneling by Kinnunen et al.[29], a high-energy peak was obtained in the low temperature limit. The difference between the result obtained in Ref. [29] and ours (Figs. 16 and 17) thus seems largely due to the difference in the spatial profile of the composite order parameter $\tilde{\Delta}(r)$ used in the two calculations.

As shown in Fig. 18 and the discussion above, the rf-tunneling current $I_F(\omega)$ is very sensitive to the detailed spatial structure of $\tilde{\Delta}(r)$. This is simply because the factor ω^{-2} in $I_F(\omega)$ [see Eq. (7.16)] tends to emphasize the role of the low energy excitations of the superfluid gas. To extract information about the high-energy region and the magnitude of $\tilde{\Delta}(0)$ in the center of the trap, it is useful to consider the function $\tilde{I}_F(\omega) \equiv \omega^2 I_F(\omega)$. In a uniform gas, when we neglect the energy dependence of the normal state density-of-states $\rho(\omega)$ for simplicity, we find that $\tilde{I}_F(\omega) \propto \Theta(\omega - |\tilde{\Delta}|)$, so that one can directly determine the magnitude of $\tilde{\Delta}$ from the energy at which the spectrum shows a sudden jump. Using the LDA, this discontinuity at $\omega = |\tilde{\Delta}|$ is broadened in a trap due to the inhomogeneity of $\tilde{\Delta}(r)$. However, one can still expect that $\tilde{I}_F(\omega)$ would start to decrease from an energy of the order

of the maximum gap, since most atoms are at the center of the trap. This behavior is clearly shown in Fig. 19, where $\tilde{I}_F(\omega)$ is seen to be suppressed for $\omega \lesssim \tilde{\Delta}(r=0)$. At the center of the trap, $\tilde{\Delta}(0)$ is of the order $1.5 \sim 2\varepsilon_F$ (see Fig. 13). We conclude that a plot of $\tilde{I}_F(\omega)$ can be used to estimate the magnitude of the composite order parameter at the center of the trap, even if there is a low-energy peak in $I_F(\omega)$.

Figure 20 shows the spectrum at $T = 0$ of the molecular current $I_M(\omega)$ given by Eq. (7.13). This Bose rf-tunneling spectrum is seen to be very similar to $\tilde{I}_F(\omega)$, as defined above (see Fig. 19). In particular, we see that the frequency where the rf-spectrum starts to be suppressed corresponds quite closely to the maximum value of the order parameter $\tilde{\Delta}(r=0)$ at the center of the trap (as shown by the arrows in Fig. 20). In a *uniform* gas, one can calculate $I_M(\omega)$ explicitly,

$$I_M(\omega) = \pi t_M^2 \phi_M^2 \rho \left(\Omega = \frac{1}{2} \frac{\omega^2 - \tilde{\Delta}^2}{\omega} + \mu \right) \Theta(\omega - \tilde{\Delta}) \Theta\left(\frac{1}{2} \frac{\omega^2 - \tilde{\Delta}^2}{\omega} + \mu\right). \quad (7.19)$$

Thus in a uniform gas, we find that $I_M(\omega) \propto \tilde{I}_F(\omega)$, since the factor ω^{-2} in Eq. (7.16) is not present in $I_M(\omega)$. Thus, measuring the molecular dissociation current $I_M(\omega)$ would appear to give a more direct way of probing the spectrum of the high energy excitations, and hence the magnitude of the composite order parameter $\tilde{\Delta}(r=0)$. In recent discussions[56], a general expression for the molecular tunneling current was discussed, but it was not evaluated in Ref.[29]. This neglect was justified by the assumption that in the BCS region of interest, the number of molecules was small. For a broad Feshbach resonance considered in Ref. [29], this may be correct but further studies are needed.

Since we can eliminate the effect of low-energy excitations on the rf-spectroscopy and extract the information about $\tilde{\Delta}(0)$ by considering $\tilde{I}_F(\omega)$ and $I_M(\omega)$, it is interesting to see where this “hidden peak” *coming from this high-energy contribution* is in the spectrum of $I_F(\omega)$ in cases where it may be masked by the low energy spectral weight (as in Fig. 16). For this purpose, we can simply model the $\tilde{I}_F(\omega)$ spectrum using the Lorentzian form

$$\tilde{I}_F(\omega) = \frac{C\omega^2}{(\omega - \omega_p)^2 + \Gamma^2}. \quad (7.20)$$

The parameters C , Γ , and ω_p can then be determined from the best fit to the calculated $\tilde{I}_F(\omega)$ *around the high-energy region* $\omega \sim \tilde{\Delta}(0)$. As an example, such a fit is shown by the dashed line in Fig. 19. The corresponding rf-tunneling spectrum $I_F(\omega)$ is shown by the dashed line in Fig. 16(b). The energy of the “hidden” broad peak in $I_F(\omega)$ is given by the

value of ω_p found by this procedure. The results for ω_p using this procedure are plotted in Fig. 21. We find reasonable agreement with the experimental data for ${}^6\text{Li}$ [27], especially for the case $\bar{U} = 0.35\varepsilon_F$. Our peak energy at $(k_F a_s)^{-1} = 0$ occurs at $\omega \simeq 0.3\varepsilon_F$, which is in agreement with the results of the recent theoretical analysis using the LDA by Törmä and co-workers[29], who found a broad peak at $\omega \sim 0.3\varepsilon_F$ near the unitarity limit. We also recall that the calculation in Ref. [29] were for a broad resonance. It would be very useful to have the calculations in Ref. [29] extended to cover the whole crossover region (results were only reported for $\nu = 0.5\varepsilon_F$).

In the recent rf-spectroscopy data at finite temperatures of Grimm and co-workers[27], one finds a strong narrow peak at zero detuning as well as a broad peak at positive detuning. As the temperature decreases, the spectral weight shifts to the broad peak. It is argued in Ref. [27] that the peak at zero detuning is due to unpaired or free Fermi atoms at the edge of the trap, which have no energy gap. The fact that the peak is narrow is further argued to be evidence that these states come from the region of low density, consistent with negligible mean-field broadening. The pioneering theoretical work of Törmä and co-workers based on the LDA[29] leads to the same interpretation. However, as discussed at the end of Sec. V, the LDA at finite temperatures incorrectly predicts a region at the edge of the trap where the order parameter $\tilde{\Delta}(r)$ has vanished even though the density of atoms $n(r)$ is still finite (see Fig. 1 of Ref. [29]). In fact, the BdG equations show that the *entire* trapped gas is in a superfluid state below T_c , with $\tilde{\Delta}(r)$ being finite everywhere where $n(r)$ is finite.

As we discussed in Section VI, very low energy states (with a finite but small excitation gap E_g) arise which are localized in the low density tail of the superfluid gas, the analogue of Andreev states[52, 57]. These in-gap surface states[55, 58] are a true signature of the Fermi superfluid phase, since they involve a coherent mixture of particle and hole components[52]. In particular, these excitations exist even at $T = 0$. At finite temperatures below T_c , the rf-tunneling current $I_F(\omega)$ involves two contributions, coming from thermally excited Bogoliubov quasi-particles and from the Cooper-pair condensate. The former contribution disappears at $T = 0$, because all the atoms are paired and Bose-condensed, and there are no excitations. However, the latter contribution exists even at $T = 0$.

The low-energy rf-current spectrum $I_F(\omega)$ is in fact dominated by excitations from the condensate associated with the low-energy Andreev or in-gap states. Indeed, we can clearly see the *true* very small excitation gap $E_g \ll \varepsilon_F$ from the lowest energy peaks in panels (a)

and (b) of Fig. 16. Törmä and co-workers[29] have argued that the normal phase atoms at the trap edge in their LDA calculation can be viewed as a crude approximation to these in-gap low energy states, which arise in a more accurate theory based on the BdG equations. However, in an LDA analysis, the low frequency (free atom) peak is predicted to disappear at very low temperatures when the entire trapped gas becomes superfluid. This picture is different from what our microscopic calculations give, as discussed above. For the same reason, we feel that the data in Ref. [27] does not give any convincing evidence for the pseudogap phase discussed in Refs. [43, 45].

A proper discussion of the low energy states in the edge of a trapped superfluid gas requires the kind of microscopic calculations presented in this paper. One is losing a huge amount of physics by thinking of the central peak (at zero detuning) simply as the contribution from unpaired atoms (or atoms feeling the effect of a “pseudogap”). This low energy peak at $\omega \ll \varepsilon_F$ is due to the characteristic low energy states ($\sim E_g \ll \varepsilon_F$) of a trapped superfluid gas in the BCS region (see Fig. 10). The BEC region is quite different. We recall from Fig. 11 that E_g rapidly increases as we pass from the BCS to the BEC regions. In the BEC region, the large energy gap E_g is determined by the magnitude of the chemical potential, rather than the low energy Andreev in-gap states. It would be very useful to attempt a higher resolution study of the “unshifted peak” in the rf-induced current measurements as presented in Ref. [27]. This could give more detailed information about the low-energy in-gap excitations of a trapped Fermi superfluid in the BCS region.

VIII. CONCLUDING REMARKS

In this paper, we have presented a detailed study of the equilibrium properties and single-particle excitations in the BCS-BEC crossover regime of a trapped Fermi gas with a Feshbach resonance, at $T = 0$. We extended the crossover theory developed by Leggett[9] to include the effect of a Feshbach resonance in a trapped Fermi gas. In our work, the composite order parameter $\tilde{\Delta}(r)$, the atomic density profile $n_F(r)$, and the chemical potential μ are all calculated self-consistently. Our theory does not use the LDA, but works with the correct eigenstates of the harmonic trapping potential given by the Bogoliubov-de Gennes (BdG) coupled equations. In a uniform BCS Fermi superfluid, the single-particle excitations have an energy gap which is equal to the pair potential Δ . In contrast, in the BCS-BEC crossover

region, this single-particle energy gap is not directly proportional to the pair potential $\tilde{\Delta}$. In a trapped Fermi superfluid, there is never a simple relation between the energy gap E_g and the underlying spatially varying order parameter $\tilde{\Delta}(r)$. One of the themes of our paper is how to extract information about both these quantities.

We showed that spatially-dependent local density and the order parameter become more localized at the center of the trap as one decreases the threshold energy (2ν) of the Feshbach resonance. This reflects the fact that the character of the particles is continuously changing, from unpaired Fermi atoms to bound states (molecules) associated with the Feshbach resonance. The threshold energy E_g of single-particle excitations was shown to be much smaller than the magnitude of composite order parameter at the center of the trap in the crossover region, where $\tilde{\Delta}(r=0) \sim \varepsilon_F$. This is because E_g in this region is determined by the lowest Andreev (or in-gap) bound states[57] near the bottom of the combined potential well composed of the off-diagonal pair potential and the trap potential. We have emphasized that these states are a characteristic signature of a trapped superfluid Fermi gas and hence are of special interest.

We also used our results for the single-particle excitation spectrum to discuss recent rf-tunneling experiments. As discussed recently[27, 29], the data at finite temperatures in the crossover region can be usefully described in terms of a narrow unshifted peak ($\omega \sim 0$) and a broad peak at a detuning frequency ω comparable to the expected pair potential $\tilde{\Delta}(r=0)$ at the center of the trap. While LDA calculations for the case $\nu = 0.5\varepsilon_F$ [29] appear to confirm this kind of rf-spectrum, our present calculations based on the explicit solutions of the BdG equations at $T = 0$ lead to somewhat different predictions about the low ω region. We have verified that our results are essentially reproduced by an LDA calculation if we base it on our self-consistent values of $n_F(r)$ and $\tilde{\Delta}(r)$ given by the BdG equations. The major difference between our results and those in Refs. [27, 29] is that we find a strong low frequency contribution to the fermionic tunneling current in the BCS-BEC crossover region. However, we find that the rf-tunneling current $I_F(\omega)$ is very dependent on the precise spatial dependence of $\tilde{\Delta}(r)$. This dependence is good news since it means that fits to the rf-tunneling data may be used in the future to obtain detailed information about the spatial dependence of the composite order parameter $\tilde{\Delta}(r)$ in the crossover region.

Further work is needed to clarify the role of the Andreev bound states in determining the low frequency peak in the rf-spectrum data. These single-particle states continue to exist

even at $T = 0$, and are clearly left out of an LDA type calculation, which is based on the results for a uniform Fermi superfluid.

In Sec. VII, we showed that the low frequency peak in the rf-spectrum was due to contribution from the edge of the trap, where $\tilde{\Delta}(r)$ is very small [see Fig. 17(b)]. Subtracting out this “surface” contribution, the remaining rf-spectrum was peaked at high energies comparable to the value of $\tilde{\Delta}(r = 0)$ at the center of the trap. These peak energies were in reasonable agreement with the observed position of the broad peak in the tunneling data reported in Ref. [27], as shown in Fig. 21.

We have also evaluated the rf-spectrum due to the current produced by dissociation of molecules (see Fig. 20) and found that it did not have an unshifted component at $\omega \sim 0$. Thus it gives a more direct measurement of $\tilde{\Delta}(r = 0)$ at the center of the trap. This contribution, which was discussed but not explicitly evaluated in Ref. [29], deserves further study, both experimentally and theoretically. In future work, we hope to extend our present calculations to finite temperatures.

Besides the single-particle properties, collective excitations in trapped Fermi superfluids[25, 28, 62] are also of great interest in the crossover region. The single-particle Green’s function evaluated in the present paper form the basis for the calculation of the collisionless collective modes in a trapped Fermi gas using linear response theory. In a future paper[36], we will extend the approach given in Ref. [3] for a uniform gas and discuss the quadrupole and monopole modes in the BCS-BEC crossover region[31]. A detailed discussion of the Kohn mode has been recently given in Ref.[63].

As discussed in Sec. VII, rf-tunneling spectroscopy experiments can give information about the true quasi-particle excitation gap E_g . However, very high resolution would be necessary in the BCS and crossover regime because $E_g \sim \omega_0 \ll \varepsilon_F$ (see Figs. 11 and 16). As a result, an interesting problem remains as to how to measure E_g in this region. An alternative method might be through the study of the collective mode frequencies, which typically have a very low energy comparable to the trap frequency ω_0 and are, in fact, bounded by the two-particle continuum at $2E_g$. We show a plot of the calculated frequency of the monopole mode in Fig. 22 (the details are discussed in Refs. [31, 36]). The monopole mode frequency is seen to be suppressed, so that it always lies below the two-particle continuum at $2E_g$. In particular, the suppression is quite striking around the region where E_g shows a minimum as a function of ν . This effect of the two-particle continuum on the monopole mode frequency

appears to be an attractive way of obtaining information about the single-particle excitation gap E_g in a trapped superfluid Fermi gas in the crossover region.

Acknowledgments

Y. O. was financially supported by a Grant-in-Aid for Scientific research from the Ministry of Education, Culture, Sports, Science and Technology of Japan, as well as by a University of Tsukuba Research Project. A. G. acknowledges a research grant from NSERC of Canada.

-
- [1] Y. Ohashi and A. Griffin, Phys. Rev. Lett. **89**, 130402 (2002).
- [2] Y. Ohashi and A. Griffin, Phys. Rev. A **67**, 033603 (2003).
- [3] Y. Ohashi and A. Griffin, Phys. Rev. A **67**, 063612 (2003).
- [4] J. N. Milstein, S. J. J. M. F. Kokkelmans and M. Holland, Phys. Rev. A **66**, 043604 (2002).
- [5] A. Perali, P. Pieri, and G. C. Striati, Phys. Rev. A **68**, 031601 (2003).
- [6] E. Timmermans, K. Furuya, P. W. Milonni and A. K. Kerman, Phys. Lett. A **285**, 228 (2001).
- [7] M. Holland, S. J. J. M. F. Kokkelmans, M. L. Chiofalo and R. Walser, Phys. Rev. Lett. **87**, 120406 (2001).
- [8] D. M. Eagles, Phys. Rev. **186**, 456 (1969).
- [9] A. J. Leggett, in *Modern Trend in the Theory of Condensed Matter* edited by A. Pekalski and J. Przystawa (Springer Verlag, Berlin, 1980), p. 14.
- [10] P. Nozières and S. Schmitt-Rink, J. Low. Temp. Phys. **59**, 195 (1985).
- [11] A. Tokumitsu, K. Miyake and K. Yamada, Phys. Rev. B **47**, 11988 (1993).
- [12] M. Randeria, in *Bose-Einstein Condensation*, edited by A. Griffin, D. W. Snoke and S. Stringari (Cambridge University Press, N.Y., 1995), p.355.
- [13] C. A. R. Sá de Melo, M. Randeria and J. R. Engelbrecht, Phys. Rev. Lett. **71**, 3202 (1993).
- [14] J. R. Engelbrecht, M. Randeria, and C. A. R. Sa de Melo, Phys. Rev. B **55**, 15153 (1997).
- [15] R. Haussmann, *Self-consistent Quantum-field Theory and Bosonization for Strongly Correlated Electron Systems* (Springer-Verlag, Berlin, 1999) Chap. 3.
- [16] T. Loftus, C. A. Regal, C. Tichnor, J. L. Bohn, and D. S. Jin, Phys. Rev. Lett. **88**, 173201 (2002).
- [17] K. Dieckmann, C. A. Stan, S. Gupta, Z. Hadzibabic, C. H. Schunck, and W. Ketterle, Phys. Rev. Lett. **89**, 203201 (2002).
- [18] C. A. Regal, C. Tichnor, J. L. Bohn, and D. S. Jin, Nature **424** (2003) 47.
- [19] K. E. Strecker, G. B. Partridge, and R. G. Hulet, Phys. Rev. Lett. **91** (2003) 080406.
- [20] M. Greiner, C. A. Regal, and D. S. Jin, Nature **426**, 537 (2003).
- [21] S. Jochim, M. Bartenstein, A. Altmeyer, G. Hendl, S. Riedl, C. Chin, J. Hecker Denschlag, and R. Grimm, Science, **302**, 2101 (2003).
- [22] C. A. Regal, M. Greiner, and D. S. Jin, Phys. Rev. Lett. **92**, 040403 (2004).

- [23] M. Bartenstein, A. Altmeyer, S. Riedl, S. Jochim, C. Chin, J. Denschlag, and R. Grimm, Phys. Rev. Lett. **92**, 120401 (2004).
- [24] M. W. Zwierlein, C. A. Stan, C. H. Schunck, S. M. F. Raupach, A. J. Kerman, and W. Ketterle, Phys. Rev. Lett. **92**, 120403 (2004).
- [25] J. Kinast, S. Hemmer, M. Gehm, A. Turlapov, and J. Thomas, Phys. Rev. Lett. **92**, 150402 (2004).
- [26] T. Bourdel, L. Khaykovich, K. Cubizolles, J. Zhang, F. Chevy, M. Teichmann, L. Tarruell, S. J. J. M. F. Kokkelmans, and C. Salomon, Phys. Rev. Lett. **91**, 020402 (2003).
- [27] C. Chin, M. Bartenstein, A. Altmeyer, S. Riedl, S. Jochim, J. Denschlag, and R. Grimm, Science **305**, 1128 (2004).
- [28] M. Bartenstein, A. Altmeyer, S. Riedl, S. Jochim, C. Chin, J. Denschlag, and R. Grimm, Phys. Rev. Lett. **92**, 203201 (2004).
- [29] J. Kinnunen, M. Rodriguez, and P. Törmä, Science **305**, 1131 (2004).
- [30] Y. Ohashi and A. Griffin, cond-mat/0402031.
- [31] Y. Ohashi, in Workshop on Ultracold Fermi Gases, Levico (Trento), Italy, March 4-6, 2004. This paper is available as a pdf-file at: <http://bec.science.unitn.it/fermi04>.
- [32] T. Kostyrko and J. Ranninger, Phys. Rev. B **54**, 13105 (1996), and references therein.
- [33] P. Pieri, and G. Strinati, Phys. Rev. B **61**, 15370 (2000).
- [34] D. Petrov, C. Salomon, and G. Shlyapnikov, Phys. Rev. Lett. **93**, 090404 (2004).
- [35] A. Griffin, *Excitations in a Bose-Condensed Liquid* (Cambridge University Press, Cambridge, 1993), Chapters 3 and 5.
- [36] Y. Ohashi and A. Griffin, in preparation; see also Ref. [31].
- [37] G. Bruun, Y. Castin, R. Dum, and K. Burnett, Eur. Phys. J. D **7**, 433 (1999)
- [38] G. Bruun, and B. R. Mottelson, Phys. Rev. Lett. **87**, 270403 (2001).
- [39] G. Bruun, Phys. Rev. Lett. **89**, 263002 (2002).
- [40] G. Bruun, and H. Heiselberg, Phys. Rev. A **65**, 053407 (2002).
- [41] P. G. de Gennes, *Superconductivity of Metals and Alloys* (Addison-Wesley, N.Y., 1966), Chapter 5; T. Tsuneto, *Superconductivity and Superfluidity* (Cambridge University Press, 1998), Chapter 3.
- [42] Since H_{HFB}^{lm} is independent of the quantum number m , we need only consider H_{HFB}^{l0} .
- [43] J. Stajic, J. Milstein, Q. Chen, M. Chiofalo, M. Holland, and K. Levin, Phys. Rev. A **69**,

- 063610 (2004).
- [44] A. Perali, P. Pieri, L. Pisani, and G. Strinati, Phys. Rev. Lett. **92**, 220404 (2004).
- [45] For a review, see Q. Chen, J. Stajic, S. Tan, and K. Levin, cond-mat/0404274.
- [46] G. D. Mahan, *Many Particle Physics, Second Edition* (Plenum Press, N.Y., 1993), Chapter 3.
- [47] J. R. Schrieffer, *Theory of Superconductivity* (Addison-Wesley, Redwood, California, 1964), Chapter 7.
- [48] See, for example, A. Fetter and J. Walecka, *Quantum Theory of Many-Particle Systems* (McGraw-Hill, N.Y., 1971), p.128ff.
- [49] We note that a_s is different from a *many-body* scattering length related to a many-body t -matrix $\Gamma(\mathbf{q}, \omega)[1]$ in the low-energy limit, defined by $4\pi a_s^{\text{mb}}/m \equiv \Gamma(\mathbf{q} = 0, \omega = 0)$. This always diverges below T_c due to the presence of the Goldstone mode at zero frequency[3].
- [50] The slight difference between the two is due to the small difference of the chemical potential determined by the equation for the total number of atoms, as shown in Fig. 2(a).
- [51] M. L. Chiofalo, S. J. J. M. F. Kokkelmans, J. N. Milstein, and M. J. Holland, Phys. Rev. Lett. **88**, 090402 (2002).
- [52] P. G. de Gennes and D. Saint James, Phys. Lett. **4**, 151 (1963).
- [53] This “excitation” energy gap is measured relative to the value of the chemical potential μ . In contrast, Fig. 3 of Ref. [30] gives a plot of $\mu + E_g$.
- [54] P. Törmä, and P. Zoller, Phys. Rev. Lett. **85**, 487 (2000).
- [55] G. Bruun, P. Törmä, M. Rodriguez, and P. Zoller, Phys. Rev. A **64**, 033609 (2001).
- [56] J. Kinnunen, M. Rodriguez, and P. Törmä, Phys. Rev. Lett. **92**, 230403 (2004).
- [57] M. Baranov, JETP Lett. **72**, 385 (2000).
- [58] H. Heiselberg, cond-mat/0406714.
- [59] D. Luxat, and A. Griffin, Phys. Rev. A **65**, 043618 (2002).
- [60] C. Choi, Y. Japha, and K. Burnett, Phys. Rev. A **61**, 063606 (2000).
- [61] This value of the excitation threshold is rather larger than $E_g \simeq 0.04\varepsilon_F$ given in Fig. 11. The difference is simply due to the fact that the threshold energy ($\equiv E_{\text{th}}$) in the tunneling current $I_F(\omega)$ is determined by $E_{\text{th}} = \text{Min}[\xi_{nl}^F + E_{jl}^F] = \text{Min}[\xi_{nl}^F] + E_g$, under the condition that energy of the Ψ_a -state [$\xi_{nl}^F = \hbar\omega_0(2n + l + 3/2) - \mu$] is positive. In panel (a) of Fig. 16, the chemical potential is $\mu = 27.56\omega_0$. Choosing the state with quantum numbers (n, l) such that $2n + l = 27$, $\text{Min}[\xi_{nl}^F] \simeq 0.94\omega_0 \simeq 0.03\varepsilon_F$. This gives a tunneling threshold energy

$E_{\text{th}} = E_g + \text{Min}[\xi_{nl}^F] \simeq 0.04\varepsilon_F + 0.03\varepsilon_F = 0.07\varepsilon_F \simeq 0.08\varepsilon_F$ in agreement with Fig. 16(a).

[62] H. Heiselberg, cond-mat/0409077; references to the literature are given here.

[63] Y. Ohashi, cond-mat/0407379; Phys. Rev. A, in press.

FIG. 1: (a) Superfluid transition temperature T_c as a function of the scattering length $(k_F a_s)^{-1}$ for a *uniform* gas. The solid line shows the case of a *narrow* Feshbach resonance ($g_r \sqrt{n} \lesssim \varepsilon_F$), while the dashed line is for the case of a *broad* Feshbach resonance ($g_r \sqrt{n} \gg \varepsilon_F$), where n is the density of atoms. The peak structure around $(k_F a_s)^{-1} \sim 0.25$ is an artifact of the approximation and is not intrinsic[15]. The solid circle shows T_c as a function of the *two-particle* scattering length a_s^{2b} in the case of $g_r \sqrt{n} = 20\varepsilon_F$ (broad Feshbach resonance). We take the cutoff $\omega_c = 2\varepsilon_F$. (b) The number of Fermi atoms N_F and the number of Bose molecules N_M at T_c in the BCS-BEC crossover. (N_M includes both Cooper-pairs and real two-body molecules.) The total number of particles is given by $N = N_F + 2N_M$. Irrespective of whether one is dealing with a broad or narrow Feshbach resonance, one notes that bound states (N_M) become dominant when $(k_F a_s)^{-1} \gtrsim 0$.

FIG. 2: (a) Chemical potential in the BCS-BEC crossover for a *uniform* gas at T_c , based on Ref. [1]. The parameters are the same as in Fig. 1. Panels (b) and (c) show detailed character of particles at T_c for a uniform gas in the cases of a narrow Feshbach resonance and broad Feshbach resonance, respectively. $N_B^{\gamma>0}$ is the number of Feshbach molecules with a finite lifetime, and $N_B^{\gamma=0}$ is the number of stable Feshbach molecules. The number of stable Cooper-pairs is $N_C^{\gamma=0}$; N_C^{sc} is the contribution from the scattering states or Cooper-pairs with a finite lifetime. For precise definitions of N_B and N_C , see Ref. [1].

FIG. 3: (a) Superfluid transition temperature T_c as a function of the scattering length $(k_F a_s)^{-1}$ for a *trapped* gas. The cases of a narrow Feshbach resonance and broad Feshbach resonance are respectively shown by the solid line and dashed line, respectively. In this figure, $n \equiv N/R_F^3$, and we take the cutoff $\omega_c = 2\varepsilon_F$. (b) The number of Fermi atoms N_F and the number of Bose molecules N_M at T_c in a harmonic trap.

FIG. 4: (a) Comparison between the bare attractive interaction $-U_{\text{eff}}$ between Fermi atoms in the gap equation [as defined in Eq. (2.10)] and the interaction $4\pi a_s/m$ defined in Eq. (4.7). We take the cutoff frequency $\omega_c = 161.5\omega_0$ and the Fermi energy $\varepsilon_F = 31.5\omega_0$ in this and later figures. (b) Relation between the scattering length a_s and the bare threshold energy 2ν , for the parameters we use in this paper. The Feshbach coupling strength is taken as $\bar{g}_r = 0.2\varepsilon_F$.

FIG. 5: Density profile in the BCS-BEC crossover. $n_F(r)$ and $n_M(r)$ represent the Fermi atom density and Bose molecule density, respectively. $n(r) = n_F(r) + 2n_M(r)$ is the total density profile. r is normalized by Thomas-Fermi radius $R_F = \sqrt{2\varepsilon_F/m\omega_0^2}$ for a free Fermi gas in a trap. We take $\bar{g}_r = 0.2\varepsilon_F$, $\bar{U} = 0.35\varepsilon_F$ and $\omega_{0B} = \omega_0$. These values are also used in Figs. 6, 7, and 8.

FIG. 6: Fermi chemical potential μ in the BCS-BEC crossover at $T = 0$. The inset shows μ as a function of the threshold energy 2ν . The dashed line in the inset is the lowest energy of molecular excitation spectrum in a trap.

FIG. 7: Spatially-dependent composite order parameter $\tilde{\Delta}(r)$ in a trap in the BCS-BEC crossover. The Cooper-pair order parameter $\Delta(r)$ and molecular condensate $\phi_m(r)$ are also shown.

FIG. 8: Expansion coefficient α_n of the molecular condensate wavefunction $\phi_M(r) = \frac{1}{\sqrt{4\pi}} \sum_n \alpha_n R_{n0}^M(r)$ given by Eqs. (2.21) and (2.22). BEC in a non-interacting Bose gas corresponds to all $\alpha_n = 0$ for $n \neq 0$.

FIG. 9: Comparison of the calculated atomic density profile $n(r)$ and composite order parameter $\tilde{\Delta}(r)$. The results are normalized by the values at the center of the trap. (a) BCS regime, and (b) BEC regime. The inset compares $n(r)$ with $\tilde{\Delta}(r)^2$ in the BEC regime.

FIG. 10: Single-particle density of states (DOS) at $T = 0$. We take $\bar{g}_r = 0.2\varepsilon_F$ and $\bar{U} = 0.52\varepsilon_F$. In calculating the DOS, we have introduced a small imaginary part ($\Gamma = 0.005\omega_0$) in the eigenenergies. The fine structure in DOS is due to the discrete levels of harmonic trapping potential. The peaks are the single-particle Bogoliubov quasi-particle energies in a trapped gas. Note that $\mu < 0$ in panel (c).

FIG. 11: Single-particle excitation gap E_g appearing in the density of states $N(\omega)$ in the BCS-BEC crossover in a trap. The dashed line shows $|\mu|$ in the negative μ region $[(k_F a_s)^{-1} > 0.65]$. The region around the minimum of E_g shown in the inset is discussed in the text. We take $\bar{g}_r = 0.2\varepsilon_F$ and $\bar{U} = 0.52\varepsilon_F$.

FIG. 12: A plot of the calculated number of atoms (N_F) and molecules (N_M) at $T = 0$. The total number of atoms is given by $N = N_F + 2N_M$. We find $N_M \simeq N/2 = 10912/2$ in the negative μ region (see also Fig. 6). We take $\bar{g}_r = 0.2\varepsilon_F$ and $\bar{U} = 0.52\varepsilon_F$.

FIG. 13: Change in the maximum value of composite order parameter $\tilde{\Delta}(0)$ at the center of the trap in the crossover region.

FIG. 14: Localized density of states $N(\omega, r)$ given by Eq. (3.9) in the crossover regime. The peaks correspond to the Andreev or in-gap states. The inset in panel (b) shows the combined potential well consisting of the composite “off-diagonal” pair potential $\tilde{\Delta}(r)$ and “diagonal” trap potential measured from the chemical potential, given by $V_{\text{eff}}^{\text{trap}}(r) \equiv (V_{\text{trap}}^F(r) - \mu)\Theta(V_{\text{trap}}^F(r) - \mu)$. Actually, atoms also feel the Hartree potential $-\frac{U}{2}n_F(r)$, but this is not plotted in the inset.

FIG. 15: (a) Combined potential well formed by the off-diagonal pair-potential $\tilde{\Delta}(r)$ and the diagonal trap potential $V_{\text{trap}}^F(r)$. The combined potential is given by the sum of $\tilde{\Delta}(r)$ and $V_{\text{eff}}^{\text{trap}}(r) \equiv (V_{\text{trap}}^F(r) - \mu)\Theta(V_{\text{trap}}^F(r) - \mu)$. The low-energy states appear around the bottom of this effective potential well. (b) Simplified model of the combined potential well which gives rise to Andreev bound states[52, 57].

FIG. 16: The rf-induced current $I_F(\omega)$ in the BCS-BEC crossover region at $T = 0$. We take $\bar{g}_r = 0.2\varepsilon_F$ and $\bar{U} = 0.52\varepsilon_F$, and introduce a finite imaginary part $\Gamma = 0.5\omega_0$ to the Bogoliubov eigenstate energies to smooth out the results. The small but finite intensity at $\omega = 0$ in panels (a) and (b) is due to this imaginary part. The dashed line in panel (b) is obtained by fitting Eq. (7.20) to $\tilde{I}_F(\omega) = \omega^2 I_F(\omega)$ around $\omega \simeq \tilde{\Delta}(r = 0)$ (see Fig. 19) to extract the high-energy “hidden” peak associated with the large composite order parameter $\tilde{\Delta}(r = 0)$ at the center of the trap. The rapid oscillations in the tunneling spectrum, also seen in Figs. 19 and 20, originates from discrete quasiparticle energy levels in a harmonic trap potential.

FIG. 17: The rf-induced current $I_F(\omega)$ evaluated using the LDA. The parameters are the same as Fig. 16. In calculating the spectrum, we have used the correct values of $n_F(r)$, $\tilde{\Delta}(r)$, and μ obtained from the solutions of the BdG coupled equations. In panel (b), (1) shows the spectral contribution from the trap region $0 \leq r \leq 0.3R_F$, and (2) shows the contribution from the larger trap region $0 \leq r \leq 0.6R_F$. These results clearly show that tunneling from the low-energy surface states is the origin of the large low frequency peak. The inset in panel (b) shows the profile of the computed composite order parameter $\tilde{\Delta}(r)$ used for $\nu = 0.6\varepsilon_F$.

FIG. 18: The solid line shows the rf-induced current $I_F(\omega)$ based on the ad-hoc “broad” composite order parameter $\tilde{\Delta}(r)$ shown in the inset. This has the same maximum value $\tilde{\Delta}(0)$ at the center of the trap as the correct order parameter shown in the inset of Fig. 17(b). However, the width is broader. In this calculation, we have also used an ad-hoc broad density profile $n_F(r)$, with a width of the same order as $\tilde{\Delta}(r)$. The dashed line shows the rf-spectrum plotted in Fig. 17(b), based on the self-consistent values of $\tilde{\Delta}(r)$ and $n_F(r)$.

FIG. 19: Spectrum of $\tilde{I}_F(\omega) \equiv \omega^2 I_F(\omega)$ versus the detuning frequency ω , for $\nu = 0.6\varepsilon_F$. Parameters are the same as in Fig. 16(b). The arrow shows the value of $\tilde{\Delta}(r = 0)$ at the center of the trap. The dashed line shows a fit to Eq. (7.20) around the high energy region ($\omega \sim \tilde{\Delta}(0)$).

FIG. 20: Molecular dissociation current $I_M(\omega)$ as a function of the effective detuning frequency ω . The arrow shows the value of the composite order parameter $\tilde{\Delta}(0)$ at the center of the trap. Parameters are the same as in Fig. 19.

FIG. 21: Peak energy in the rf-tunneling current. In the crossover regime ($0.2 < \mu/\varepsilon_F < 1$), the current is peaked at an energy evaluated using Eq. (7.20). The solid line shows $\tilde{\Delta}(0)$ in the case of $\bar{U} = 0.35\varepsilon_F$ (see also Fig. 13). Experimental data (open circles) are taken from Figs. 1 and 2 of Ref. [27].

FIG. 22: Calculated frequency of the monopole mode ($L = 0$ and $n = 1$) in the BCS-BEC crossover region at $T = 0$. In this figure, $2E_g$ describes the threshold of the two-particle continuum spectrum. The monopole mode is suppressed below this two-particle continuum. The collective mode frequency is obtained from the pole of density-density correction function calculated in the generalized random phase approximation[31, 36].

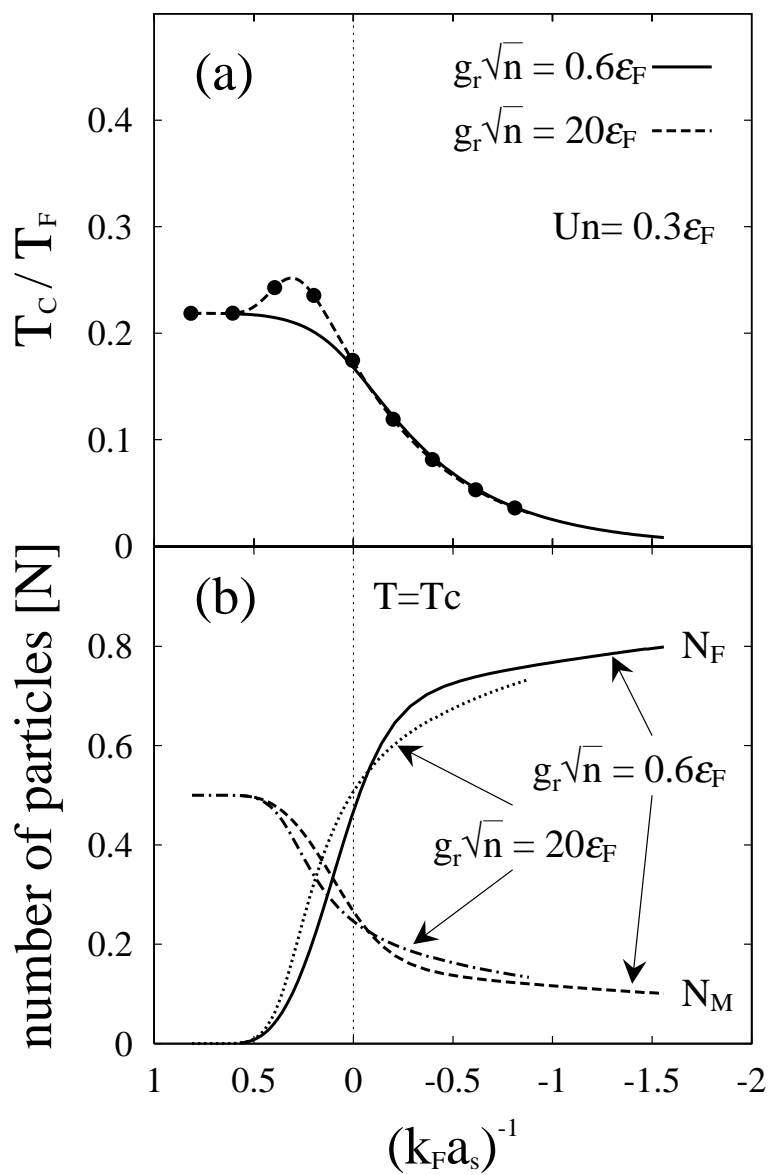


Fig.1 Ohashi and Griffin

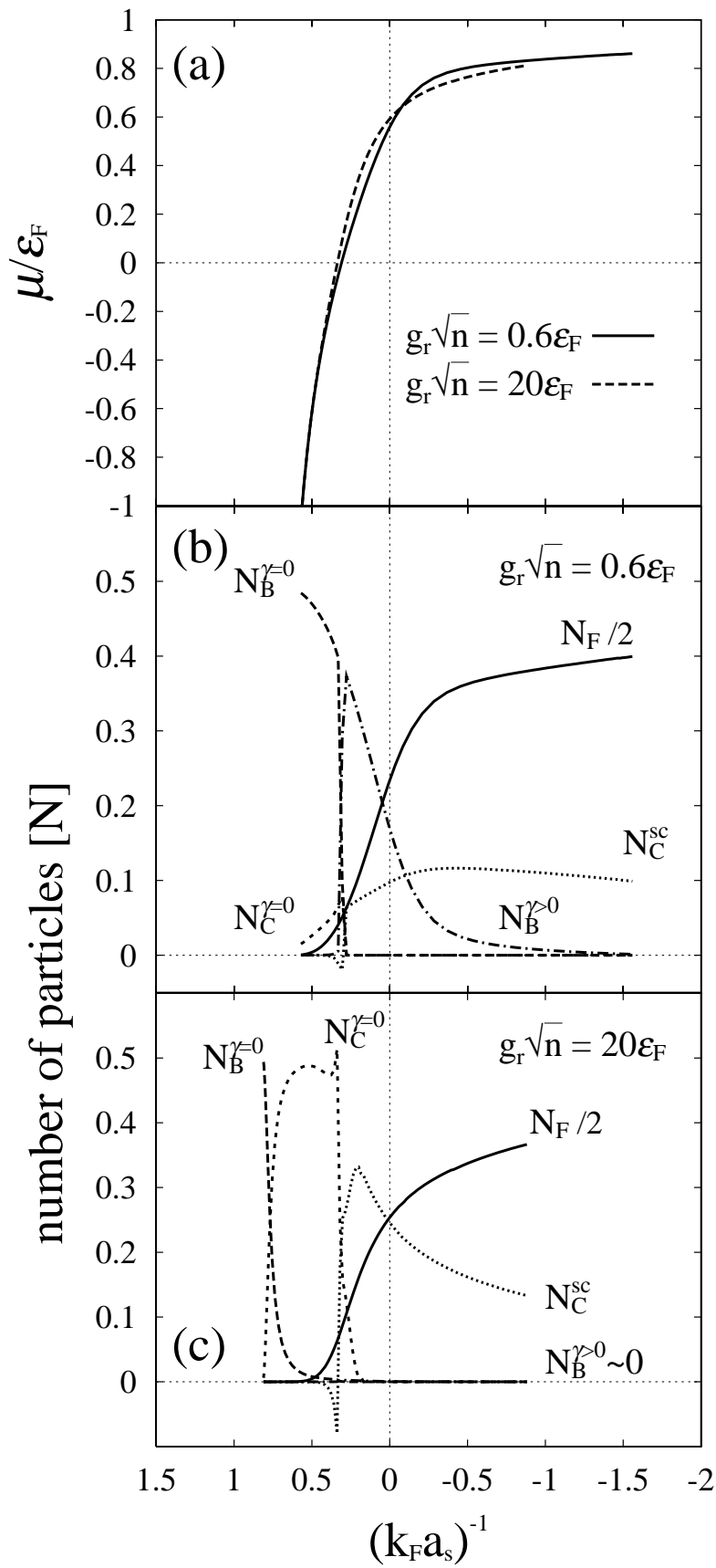


Fig.2 Ohashi and Griffin

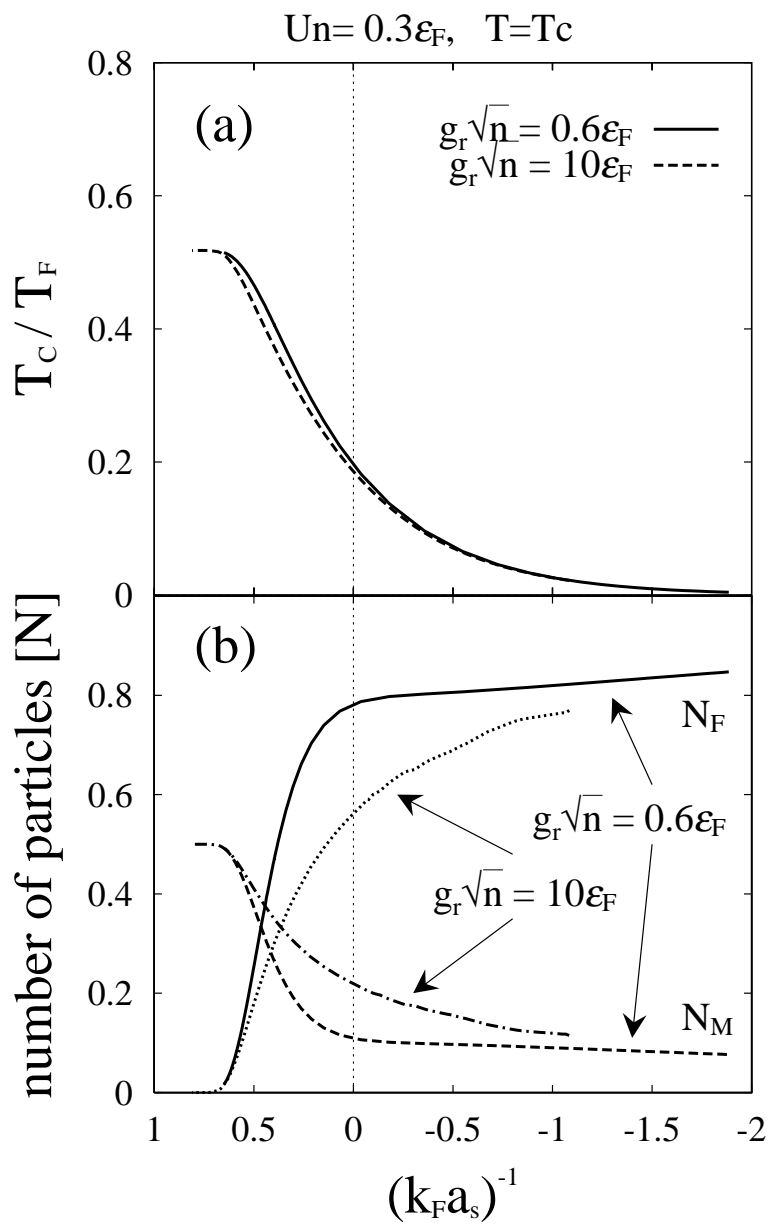


Fig.3 Ohashi and Griffin

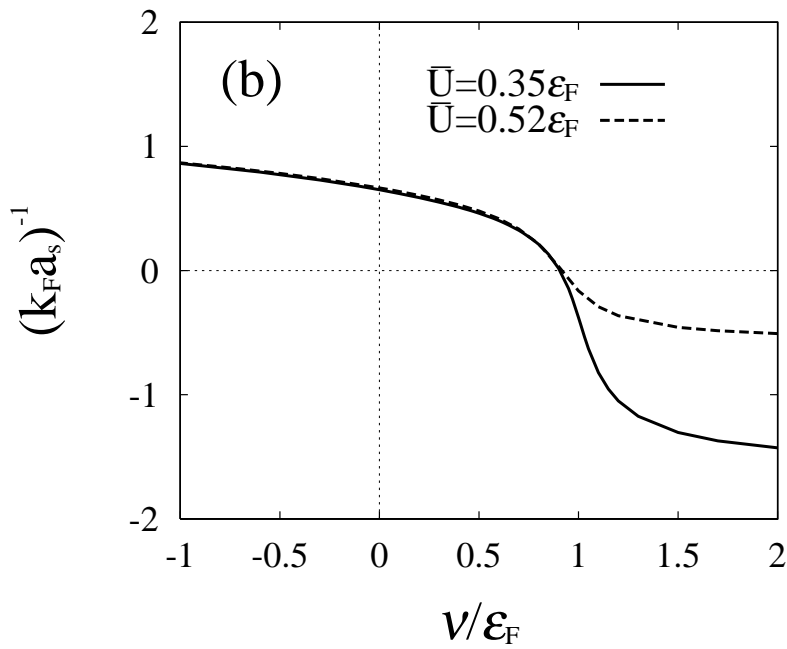
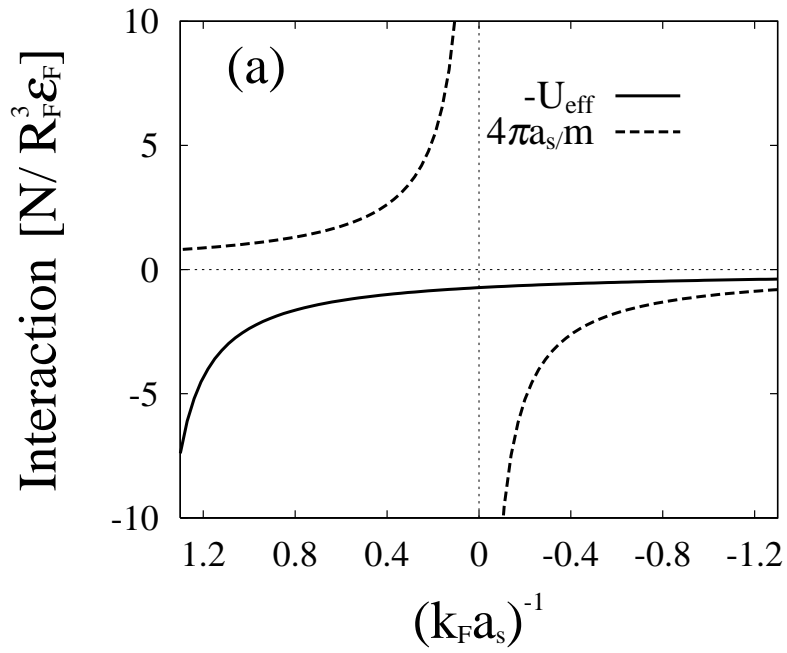


Fig.4 Ohashi and Griffin

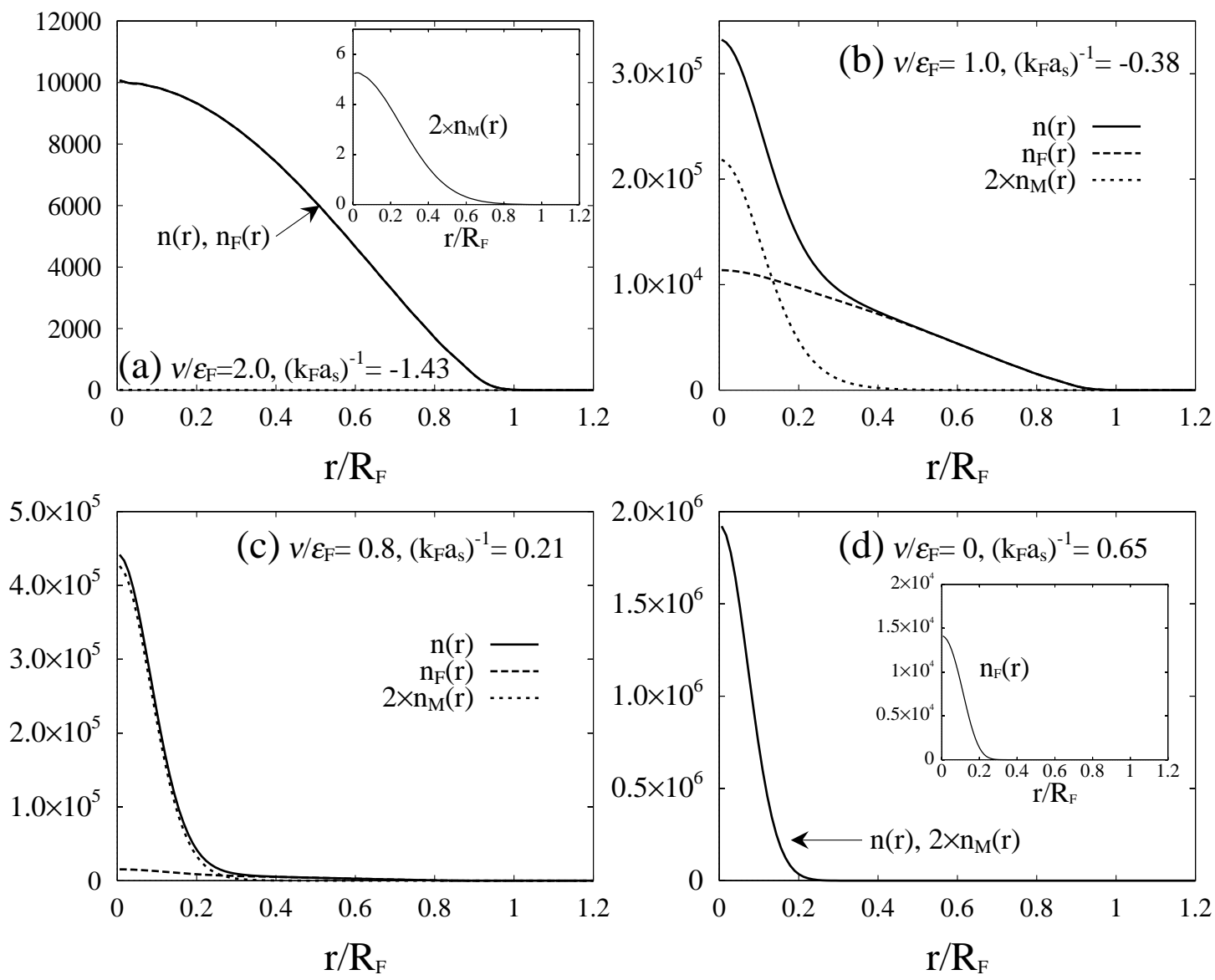


Fig.5 Ohashi and Griffin

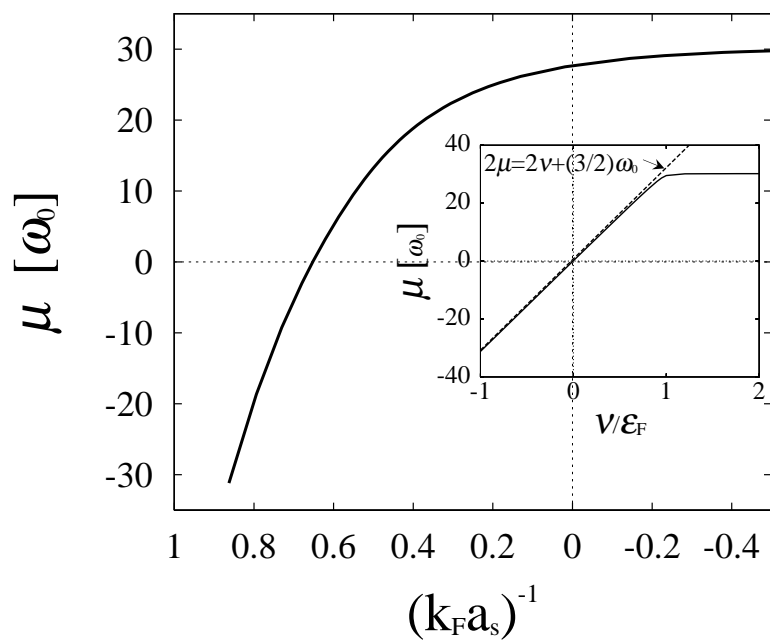


Fig.6 Ohashi and Griffin

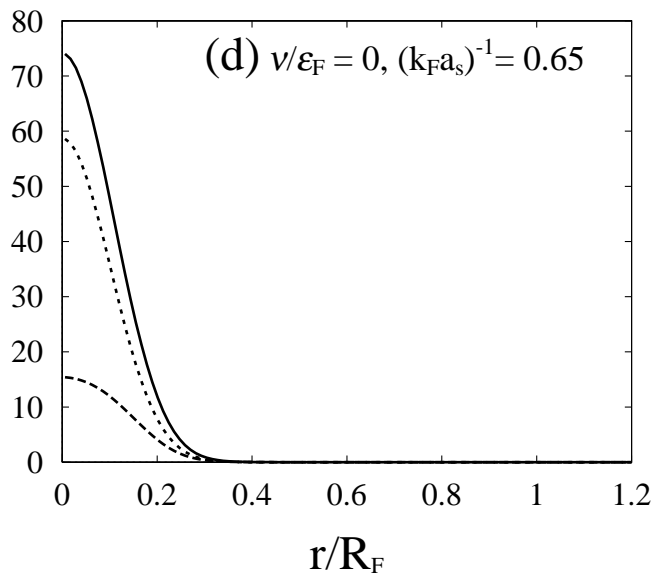
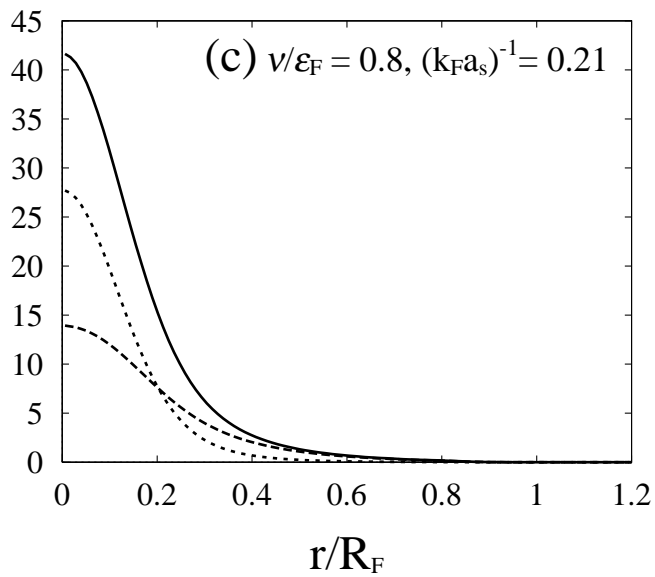
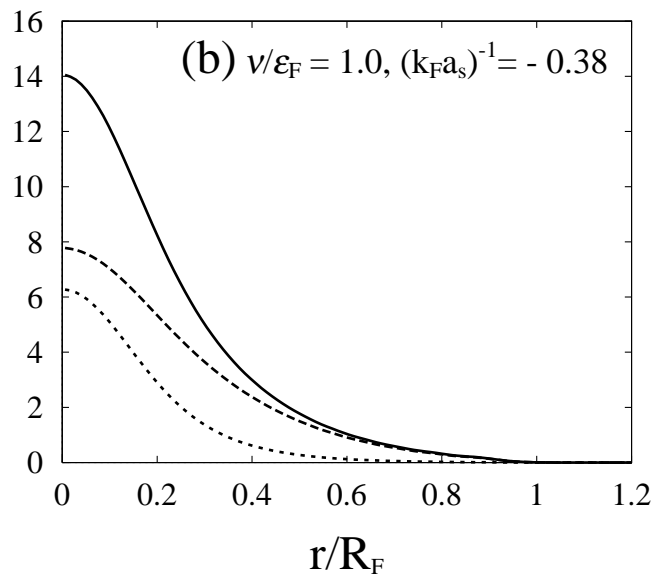
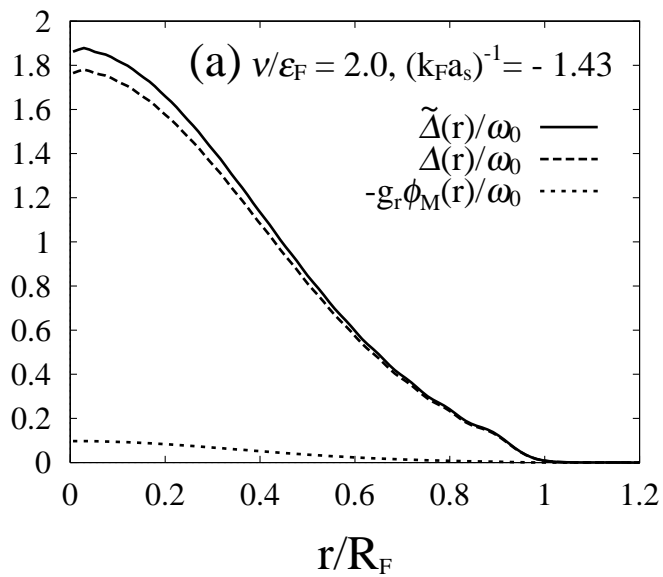


Fig.7 Ohashi and Griffin

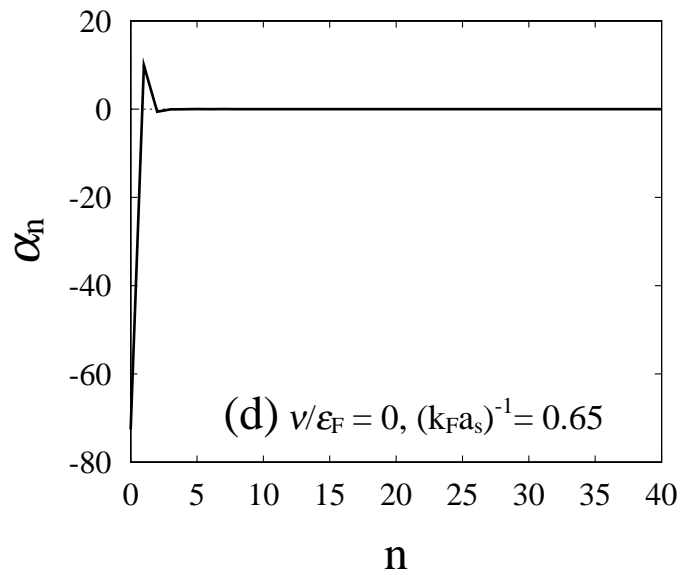
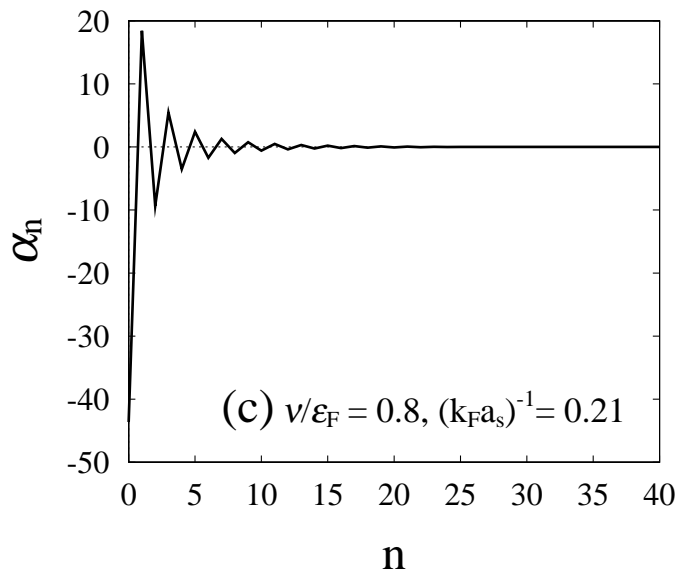
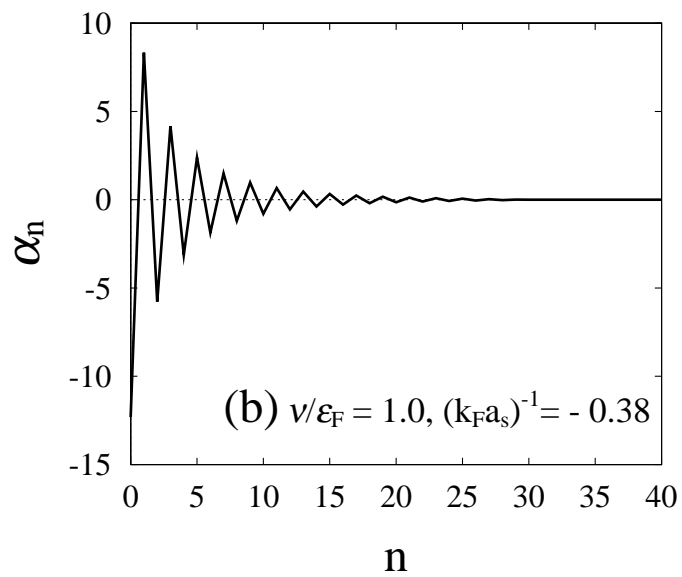
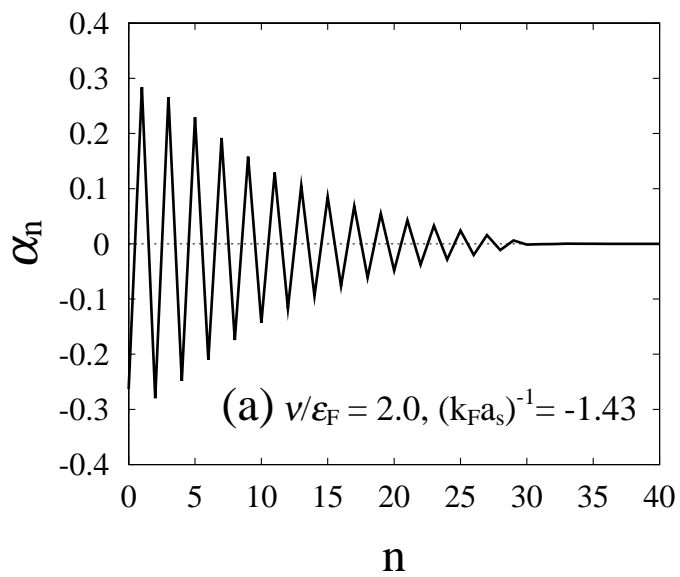


Fig.8 Ohashi and Griffin

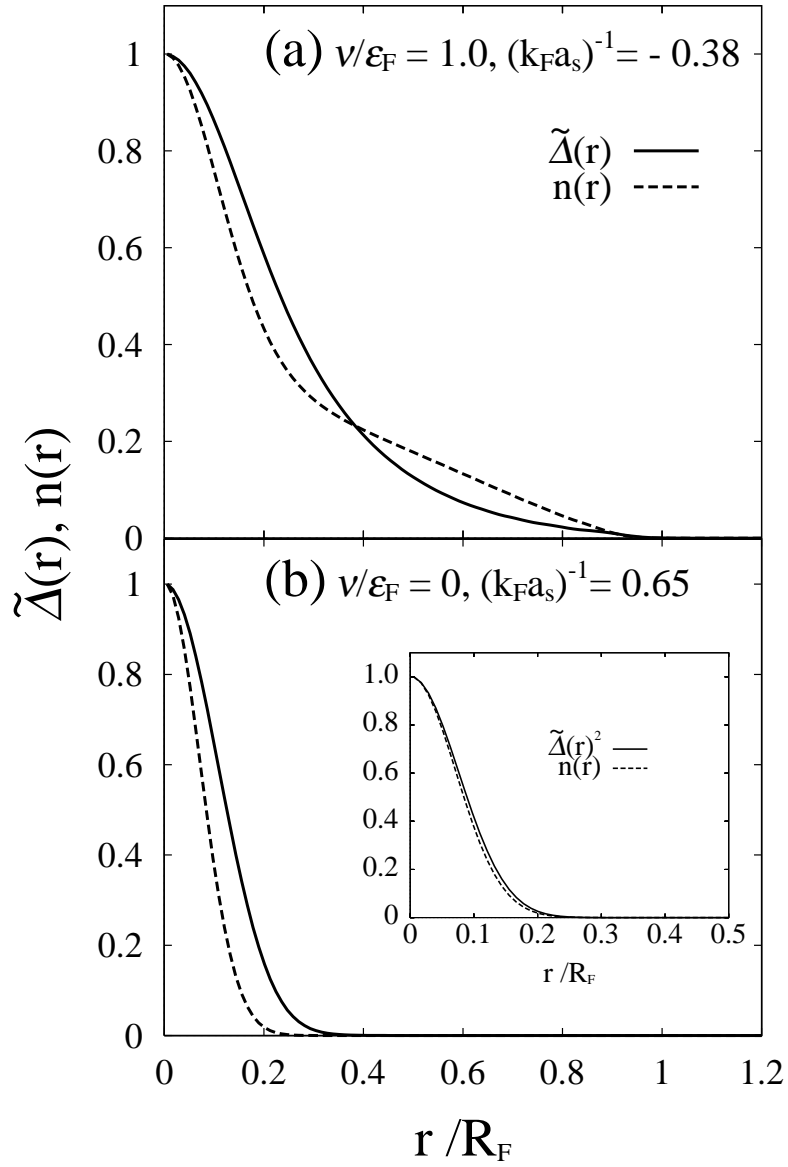


Fig.9 Ohashi and Griffin

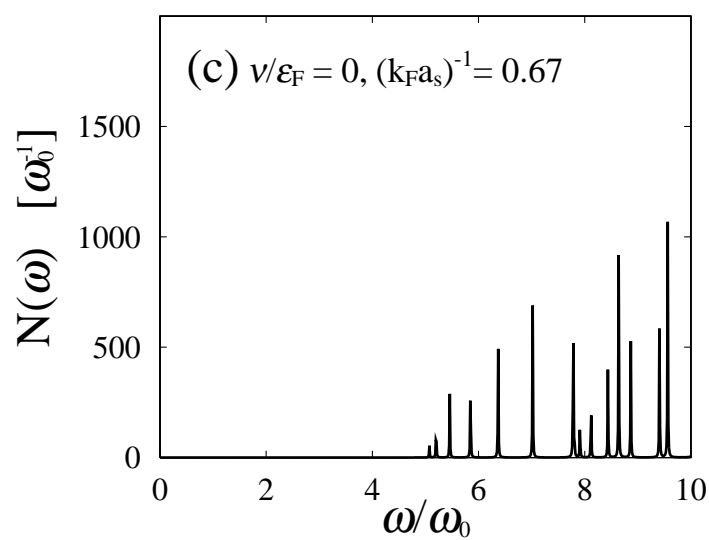
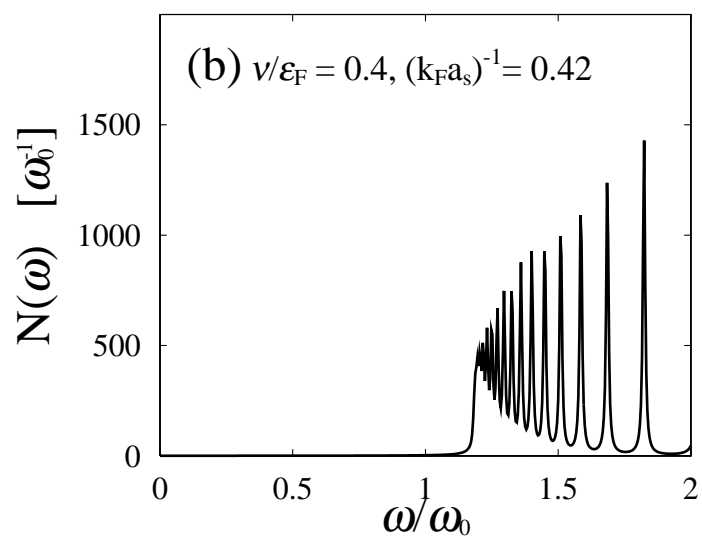
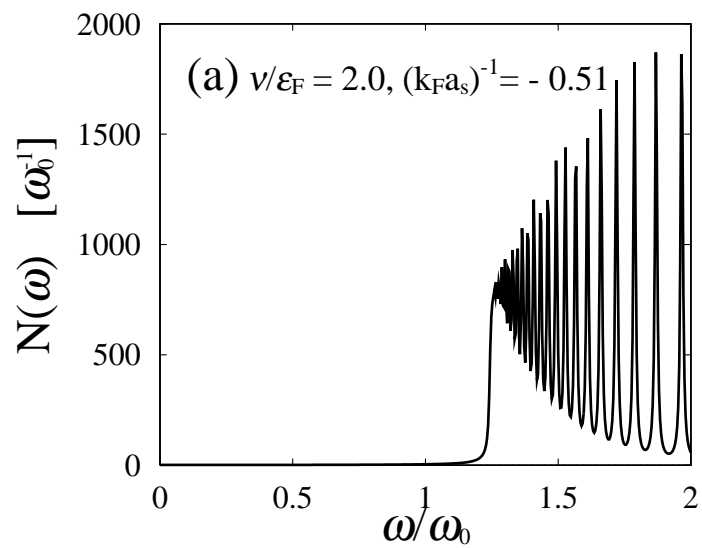


Fig.10: Ohashi and Griffin

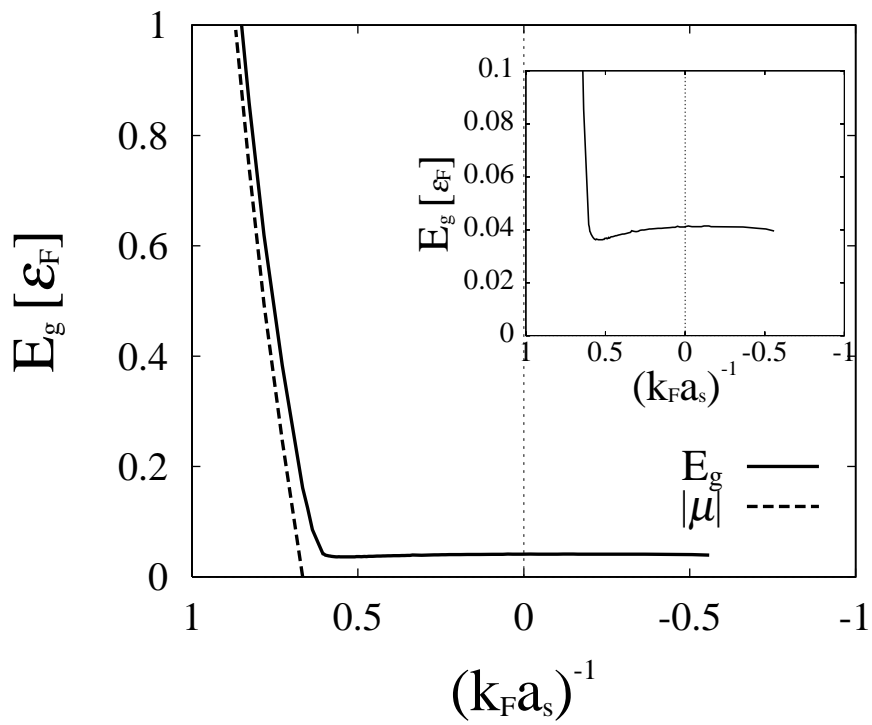


Fig.11 Ohashi and Griffin

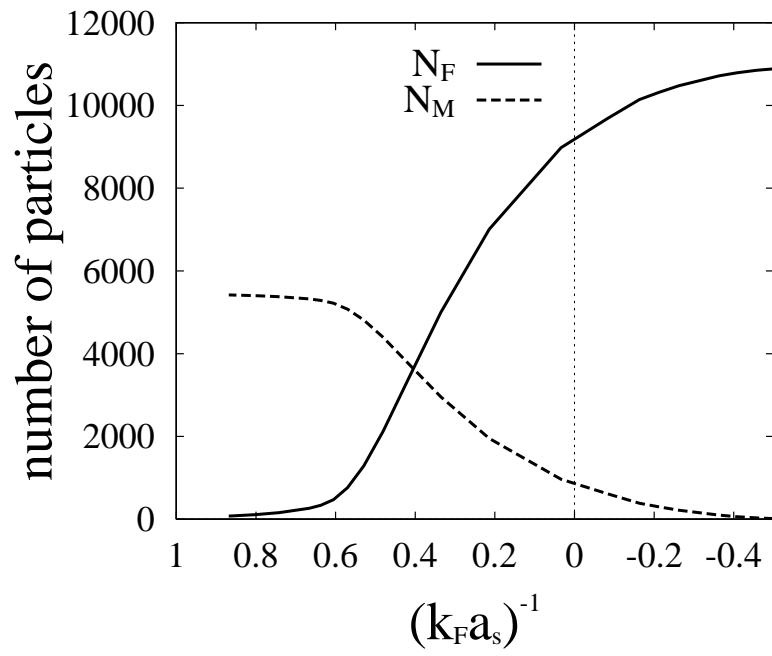


Fig.12 Ohashi and Griffin

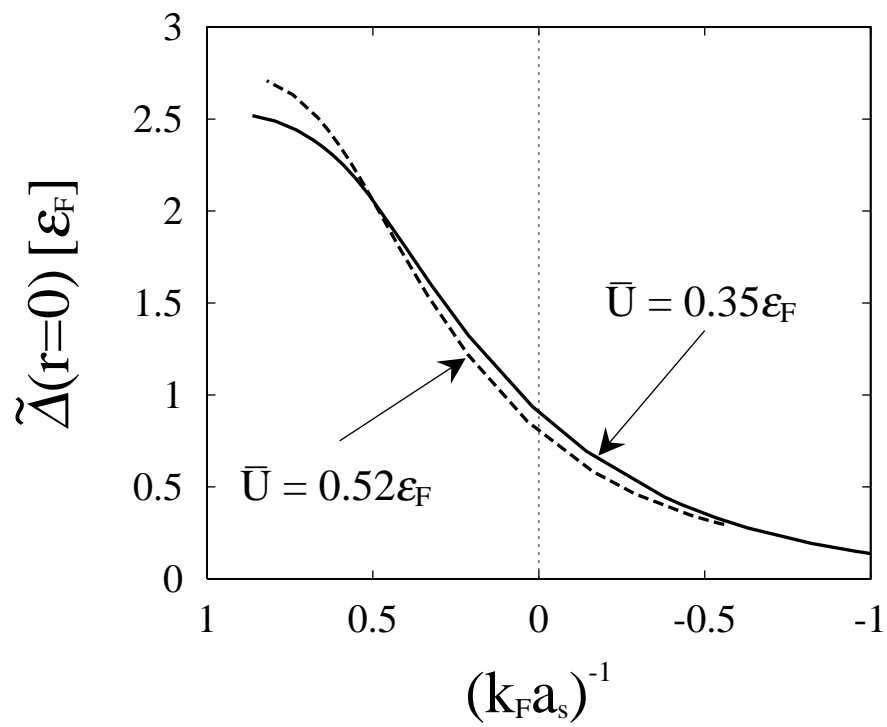


Fig.13 Ohashi and Griffin

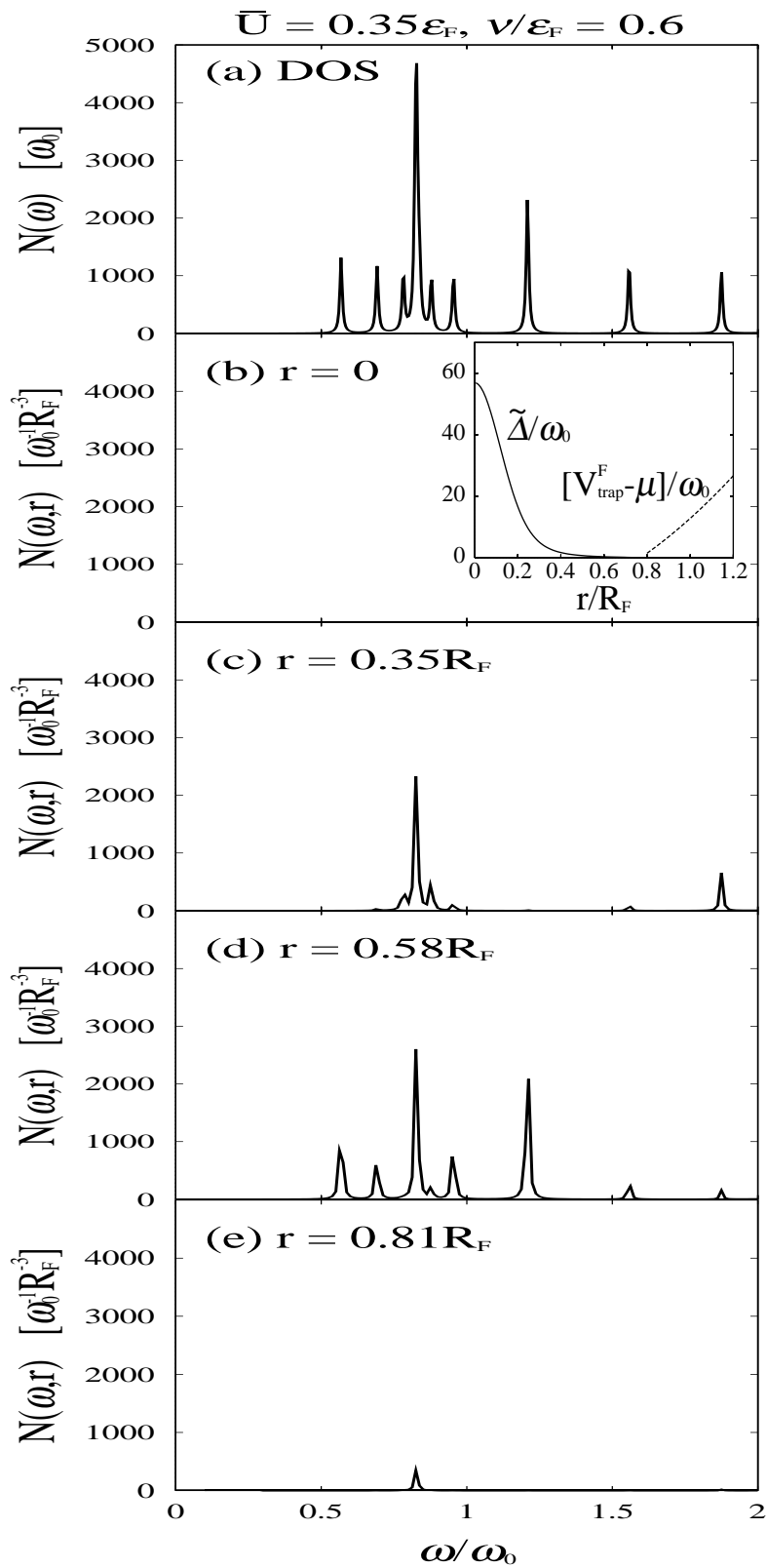


Fig.14 Ohashi and Griffin

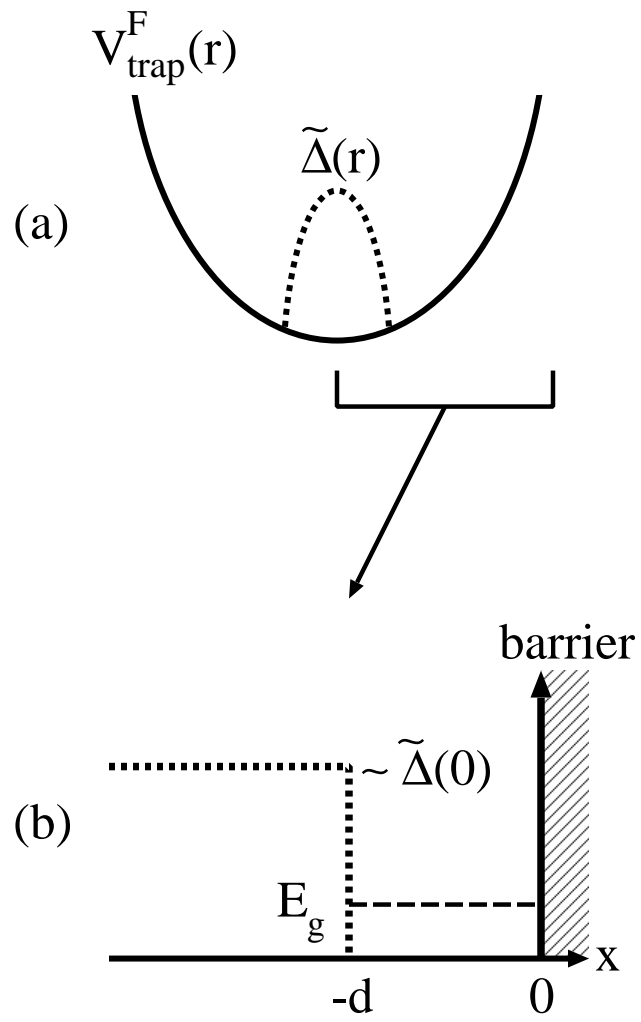


Fig.15 Ohashi and Griffin

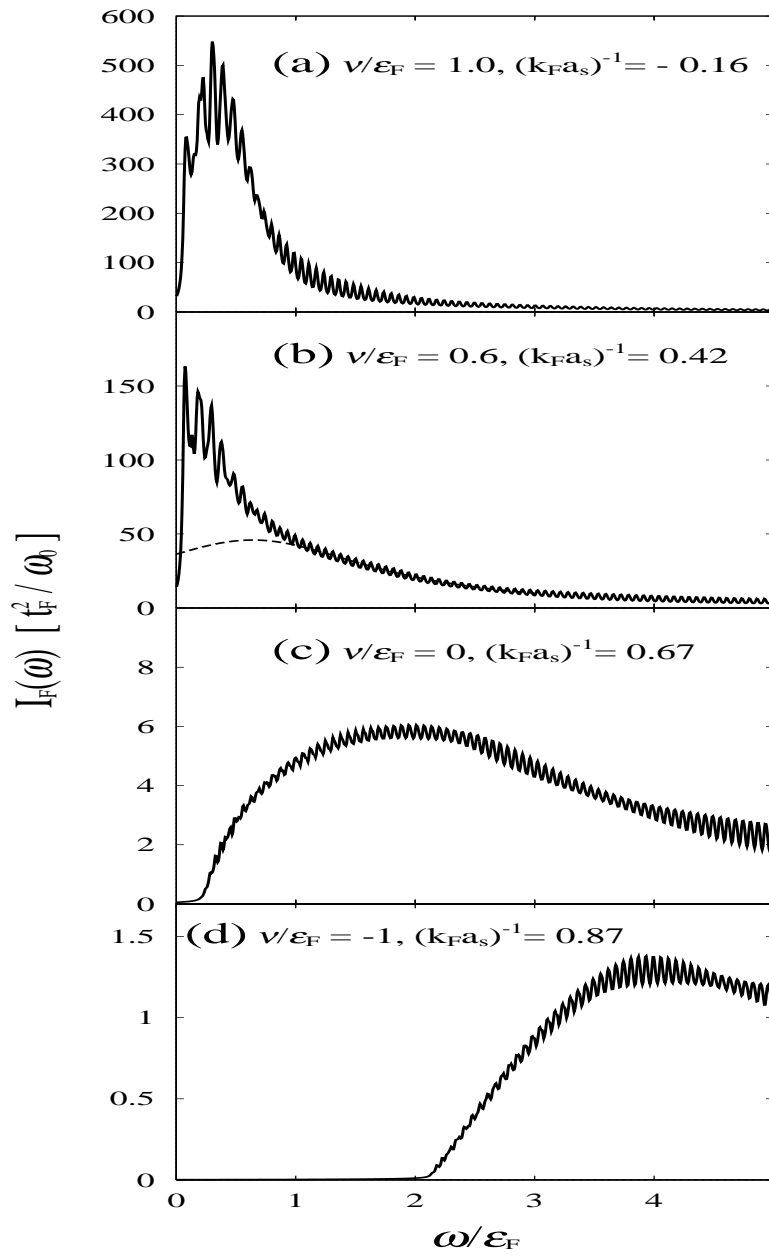


Fig.16 Ohashi and Griffin

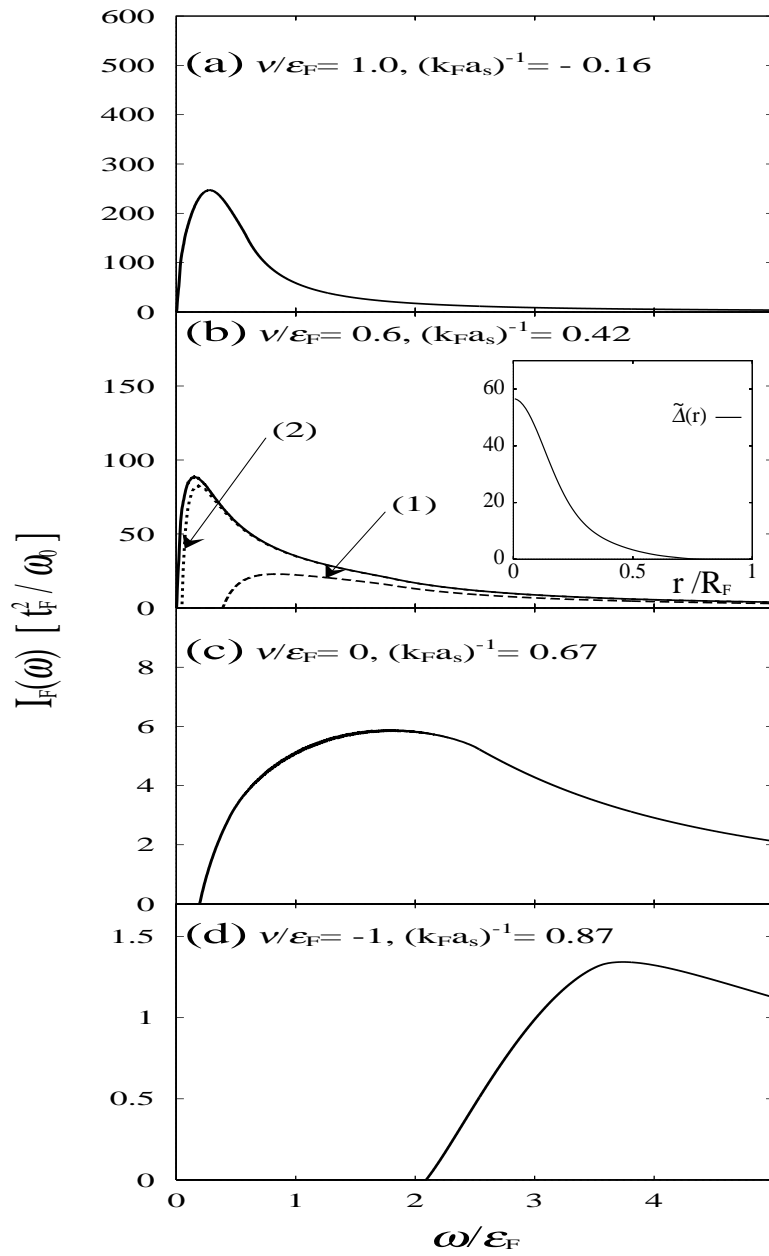


Fig.17 Ohashi and Griffin

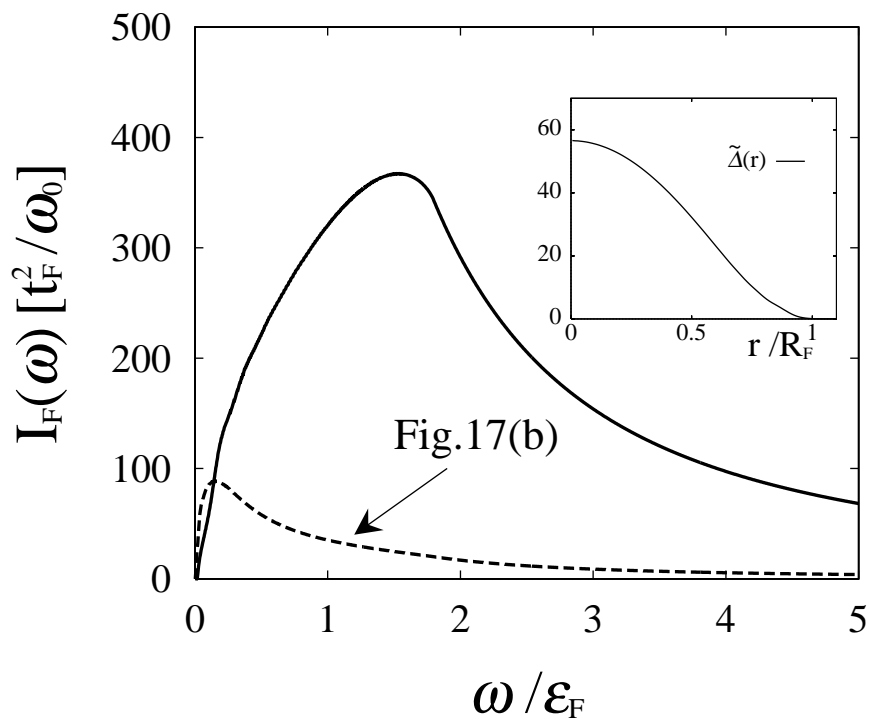


Fig.18 Ohashi and Griffin

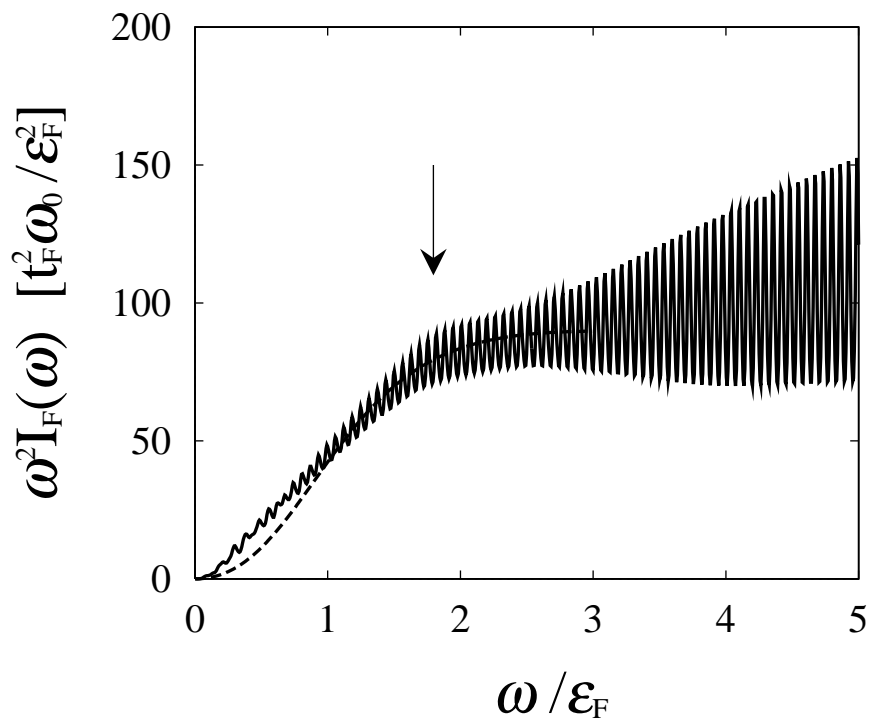


Fig.19 Ohashi and Griffin

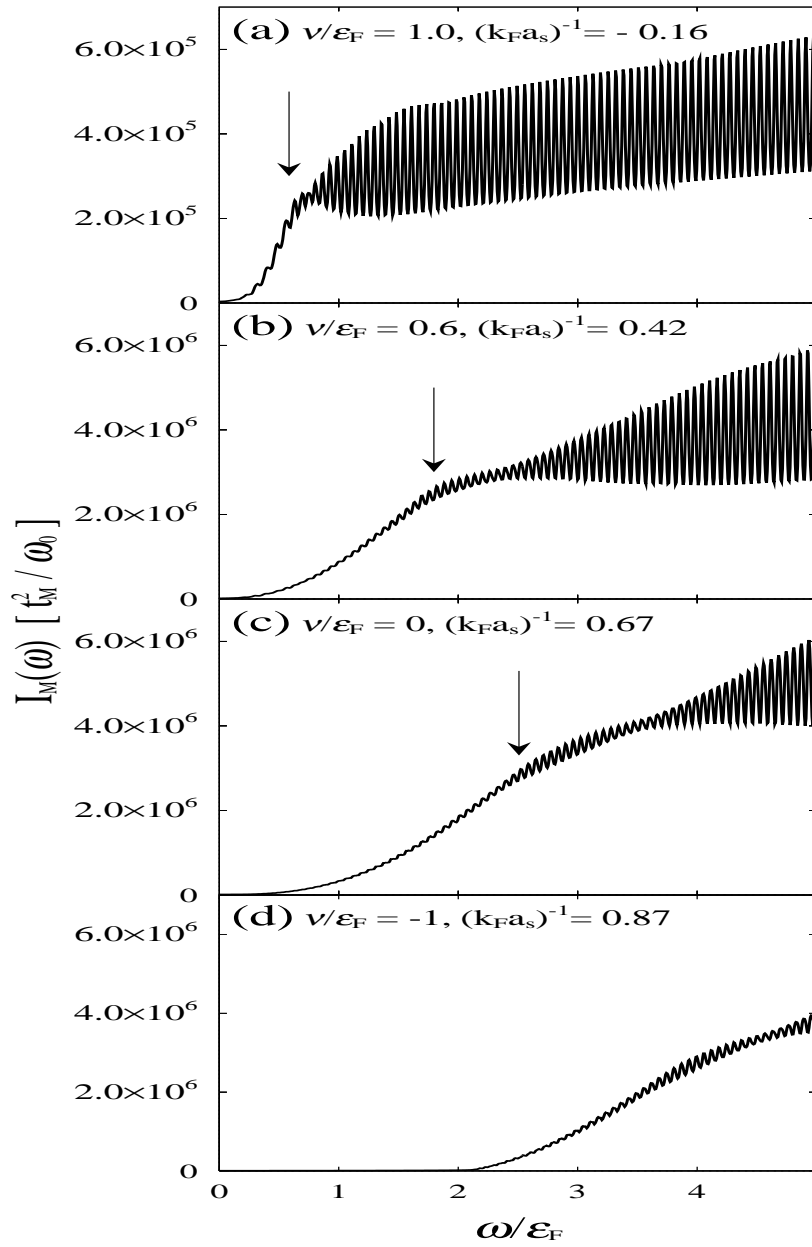


Fig.20 Ohashi and Griffin

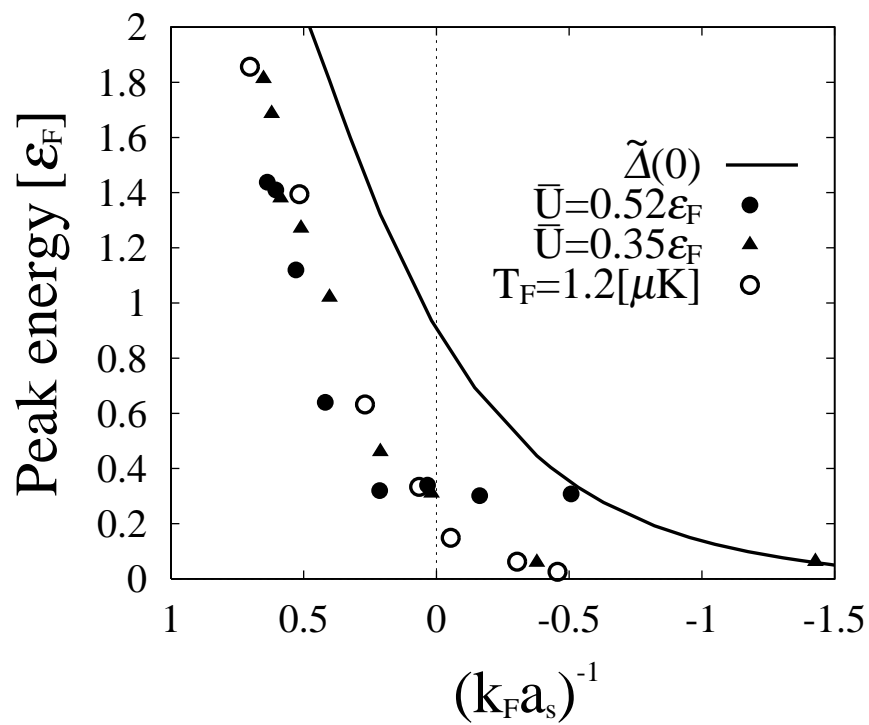


Fig.21 Ohashi and Griffin

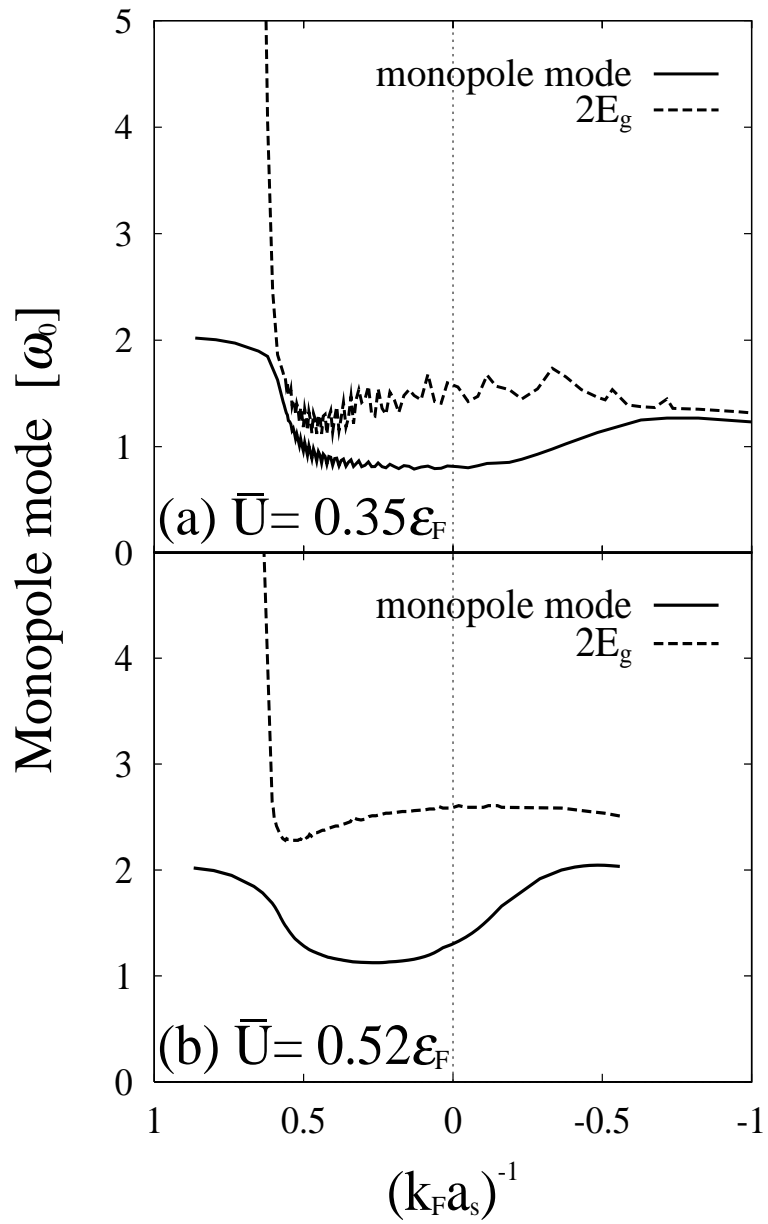


Fig.22 Ohashi and Griffin